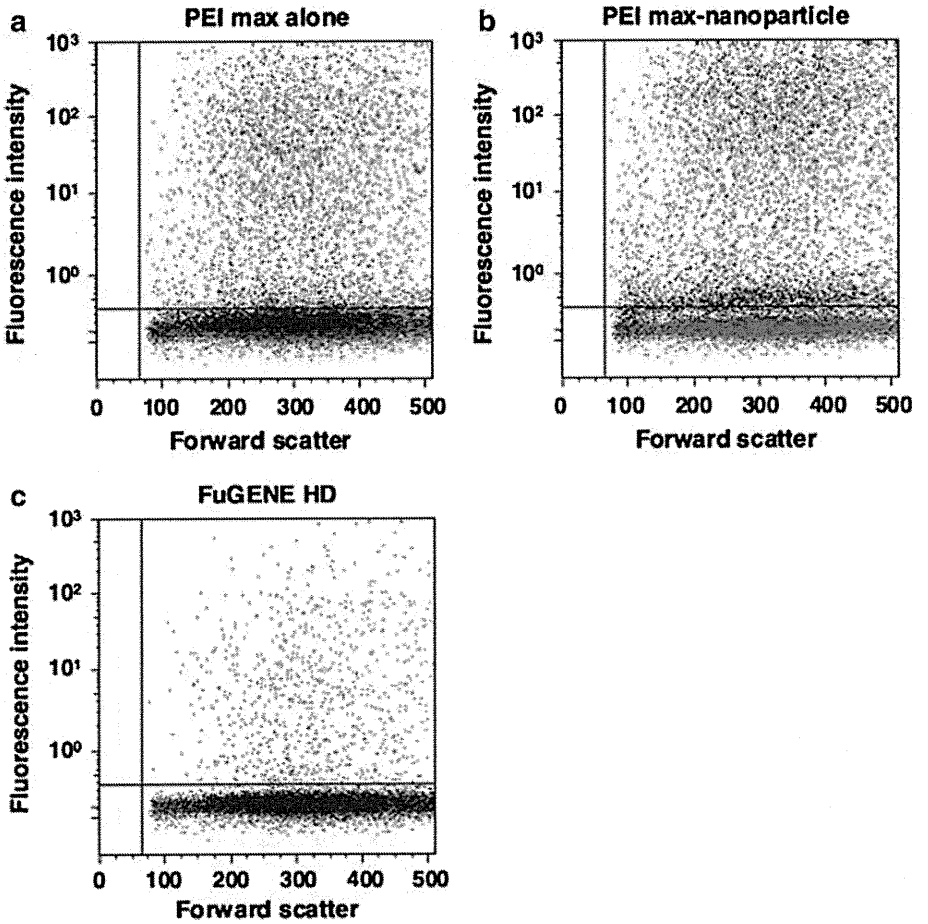

Fig. 5 Transfection efficiency of the deacylated polyethylenimine (PEI max)-nanoparticle. Comparison of scattering properties of the untreated CL6 cells (mock, *red dot*) and with PEI max alone (**a**, *blue dot*, 42.2 ± 8.5%), PEI max-nanoparticles (**b**, *blue dot*, 81.1 ± 4.0%), or FuGENE HD (**c**, *blue dot*, 13.9 ± 1.1%) by flow cytometry

Table 1 Comparison of transfection methods using the polyethylenimine and magnetic nanoparticles

Author	Year	Vector	Component	Cell	Transfection efficiency	Cell viability (% of control)	References
Kami	–	Plasmid	PEI max (MW 25k), MNP (γ-Fe2O3, 70 nm), MF (0.2 T)	P19CL6	80%[a]	100	This paper
Zhang	2010	Plasmid	Branched PEI (MW 25k), SPION (30 nm), MF (1.2 T)	NIH3T3	64%[a]	100	[14]
		siRNA	Branched PEI (MW 25k), SPION (30 nm), MF (1.2 T)	NIH3T3	77%[a]	100	
Kievit	2009	Plasmid	PEI (MW 25k), SPION (200 nm)	C6	90%[a]	10	[13]
		Plasmid	PEI (MW 25k), Chitosan, SPION (200 nm)	C6	45%[a]	100	
		Plasmid	PolyMag (commercial magnification reagent), MF (1.2 T)	C6	32%[a]	66	
Scherer	2002	Plasmid	PEI (MW 800k), SPION (200 nm), MF (1 T)	NIH3T3	5-fold[b]	–	[15]
		Adenovirus	PEI (MW 800k), SPION (200 nm), MF (1 T)	K562	100-fold[b]	–	
		Retrovirus	PEI (MW 800k), SPION (200 nm), MF (1 T)	NIH3T3	20%[a]	–	

Transfection efficiency indicates optimal transfection condition

PEI polyethylenimine, *PEI max* deacylated PEI, *MNP* magnetic nanoparticle, *SPION* superparamagnetic iron oxide nanoparticle, *MW* molecular weight, *MF* magnetic force, *T* tesla

[a] Flowcytometric analysis

[b] Luciferase activity assay

introducing plasmid into target cells with increased efficiency. Furthermore, a major advantage of this method is its tolerability among cells. Other methods might be limited either by possible cytotoxic effects of the lipidic transfection reagent (lipofection) or simply by the directly applied force on the cells (electroporation). In contrast, methods such as lipofection offer only a certain probability of hits between cargo and cells because of the three-dimensional motion of cells and transfection aggregates in a liquid suspension. Normally, transfection was inhibited

by serum using transfection reagent [25]. However, this method can also be performed in the presence of serum, which is a further benefit. Additionally, synergistic effects on transfection efficiency can arise from the possible combination of PEI max and nanoparticles. This technology might be an alternative to the currently used viral and nonviral vectors in gene therapy and gene transfer [26].

Our results suggest that PEI max-nanoparticles offer the ability to deliver various DNA formulations in addition to the traditional methods. Furthermore, gene transfer efficiency was not inhibited in the presence of serum in the cells. PEI max-nanoparticles may be a promising gene carrier with high transfection efficiency and low cytotoxicity.

Acknowledgments We express our sincere thanks to Koichiro Nishino (Department of Reproductive Biology, National Institute for Child Health and Development) for pCAGGS-EGFP. This study was supported by a Grant-in-Aid for the Global COE Program, Science for Future Molecular Systems from the Ministry of Education, Culture, Sports, Science and Technology, Japan (MEXT).

References

1. Kimura T, Iwai S, Moritan T, Nam K, Mutsuo S, Yoshizawa H, Okada M, Furuzono T, Fujisato T, Kishida A. Preparation of poly(vinyl alcohol)/DNA hydrogels via hydrogen bonds formed on ultra-high pressurization and controlled release of DNA from the hydrogels for gene delivery. J Artif Organs. 2007;10:104–8.
2. Moritake S, Taira S, Ichiyanagi Y, Morone N, Song SY, Hatanaka T, Yuasa S, Setou M. Functionalized nano-magnetic particles for an in vivo delivery system. J Nanosci Nanotechnol. 2007;7:937–44.
3. Tomitaka A, Koshi T, Hatsugai S, Yamada T, Takemura Y. Magnetic characterization of surface-coated magnetic nanoparticles for biomedical application. J Magn Magn Mater. 2010;323: 1396–1403.
4. Yokoyama M. Drug targeting with nano-sized carrier systems. J Artif Organs. 2005;8:77–84.
5. Lauterbur PC, et al. Image formation by induced local interactions. Examples employing nuclear magnetic resonance. Clin Orthop Relat Res. 1973;1989:3–6.
6. Nakamura H, Ito N, Kotake F, Mizokami Y, Matsuoka T. Tumor-detecting capacity and clinical usefulness of SPIO-MRI in patients with hepatocellular carcinoma. J Gastroenterol. 2000;35: 849–55.
7. Karlsson HL, Cronholm P, Gustafsson J, Moller L. Copper oxide nanoparticles are highly toxic: a comparison between metal oxide nanoparticles and carbon nanotubes. Chem Res Toxicol. 2008; 21:1726–32.
8. Karlsson HL, Gustafsson J, Cronholm P, Moller L. Size-dependent toxicity of metal oxide particles–a comparison between nano- and micrometer size. Toxicol Lett. 2009;188:112–8.
9. Boussif O, Lezoualc'h F, Zanta MA, Mergny MD, Scherman D, Demeneix B, Behr JP. A versatile vector for gene and oligonucleotide transfer into cells in culture and in vivo: polyethylenimine. Proc Natl Acad Sci USA. 1995;92:7297–301.
10. Wang J, Gao L. Adsorption of polyethylenimine on nanosized zirconia particles in aqueous suspensions. J Colloid Interface Sci. 1999;216:436–9.
11. Vancha AR, Govindaraju S, Parsa KV, Jasti M, Gonzalez-Garcia M, Ballestero RP. Use of polyethyleneimine polymer in cell culture as attachment factor and lipofection enhancer. BMC Biotechnol. 2004;4:23.
12. Thomas M, Lu JJ, Ge Q, Zhang C, Chen J, Klibanov AM. Full deacylation of polyethylenimine dramatically boosts its gene delivery efficiency and specificity to mouse lung. Proc Natl Acad Sci USA. 2005;102:5679–84.
13. Kievit FM, Veiseh O, Bhattarai N, Fang C, Gunn JW, Lee D, Ellenbogen RG, Olson JM, Zhang M. PEI-PEG-chitosan copolymer coated iron oxide nanoparticles for safe gene delivery: synthesis, complexation, and transfection. Adv Funct Mater. 2009;19:2244–51.
14. Zhang H, Lee MY, Hogg MG, Dordick JS, Sharfstein ST. Gene delivery in three-dimensional cell cultures by superparamagnetic nanoparticles. ACS Nano. 2010;4:4733–43.
15. Scherer F, Anton M, Schillinger U, Henke J, Bergemann C, Kruger A, Gansbacher B, Plank C. Magnetofection: enhancing and targeting gene delivery by magnetic force in vitro and in vivo. Gene Ther. 2002;9:102–9.
16. Bertram J. MATra—magnet assisted transfection: combining nanotechnology and magnetic forces to improve intracellular delivery of nucleic acids. Curr Pharm Biotechnol. 2006;7: 277–85.
17. Arsianti M, Lim M, Marquis CP, Amal R. Polyethylenimine based magnetic iron-oxide vector: the effect of vector component assembly on cellular entry mechanism, intracellular localization, and cellular viability. Biomacromolecules. 2010;11:2521–31.
18. Georgieva JV, Kalicharan D, Couraud PO, Romero IA, Weksler B, Hoekstra D, Zuhorn IS. Surface characteristics of nanoparticles determine their intracellular fate in and processing by human blood-brain barrier endothelial cells in vitro. Mol Ther. 2011; 19:318–25.
19. Longmire M, Choyke PL, Kobayashi H. Clearance properties of nano-sized particles and molecules as imaging agents: considerations and caveats. Nanomedicine (Lond). 2008;3:703–17.
20. Niwa H, Yamamura K, Miyazaki J. Efficient selection for high-expression transfectants with a novel eukaryotic vector. Gene. 1991;108:193–9.
21. Nakayama GR, Caton MC, Nova MP, Parandoosh Z. Assessment of the Alamar blue assay for cellular growth and viability in vitro. J Immunol Methods. 1997;204:205–8.
22. Namgung R, Singha K, Yu MK, Jon S, Kim YS, Ahn Y, Park IK, Kim WJ. Hybrid superparamagnetic iron oxide nanoparticle-branched polyethylenimine magnetoplexes for gene transfection of vascular endothelial cells. Biomaterials. 2010;31:4204–13.
23. Song HP, Yang JY, Lo SL, Wang Y, Fan WM, Tang XS, Xue JM, Wang S. Gene transfer using self-assembled ternary complexes of cationic magnetic nanoparticles, plasmid DNA and cell-penetrating Tat peptide. Biomaterials. 2010;31:769–78.
24. Coonrod A, Li FQ, Horwitz M. On the mechanism of DNA transfection: efficient gene transfer without viruses. Gene Ther. 1997;4:1313–21.
25. Purow BW, Sundaresan TK, Burdick MJ, Kefas BA, Comeau LD, Hawkinson MP, Su Q, Kotliarov Y, Lee J, Zhang W, Fine HA. Notch-1 regulates transcription of the epidermal growth factor receptor through p53. Carcinogenesis. 2008;29:918–25.
26. Davis ME. Non-viral gene delivery systems. Curr Opin Biotechnol. 2002;13:128–31.

J Orthop Sci (2011) 16:670–672
DOI 10.1007/s00776-011-0119-2

RAPID SHORT COMMUNICATION

Gene expression profiling of mouse growth plate cartilage by laser microdissection and microarray analysis

Honoka Isshiki · Kazuki Sato · Keisuke Horiuchi · Shuichi Tsutsumi · Makoto Kano · Hiroyasu Ikegami · Hitoshi Abe · Akihiro Umezawa · Hiroyuki Aburatani · Yoshiaki Toyama

Received: 4 April 2011 / Accepted: 9 June 2011 / Published online: 1 July 2011

Introduction

Longitudinal bone growth results from a complex sequence of events involving differentiation of resting chondroblasts into proliferative, pre-hypertrophic, and hypertrophic chondrocytes. The growth plate (epiphyseal plate), which is primarily responsible for longitudinal growth, can be divided into four distinct zones: the resting zone (RZ), proliferating zone (PZ), maturing zone (MZ), and hypertrophic zone (HZ), on the basis of the morphology of the developing chondroblasts and the structure of the cartilage matrix. In the past two decades substantial progress has been made in understanding the mechanisms underlying chondroblast differentiation and skeletal development [1–3]. However, comprehensive analysis of gene expression patterns in the growth plate has been technically challenging.

In this study, we performed a gene expression profile analysis of each zone of the growth plate from 9-day-old mice, using microdissection and microarray analysis, and determined the expression profiles of 1,995 genes in the murine growth plate. Furthermore, we have created a publicly available and searchable on-line database [murine growth plate database (MGPDB)] containing the gene expression data from this study (http://157.82.78.238/mgpdb/main_search.jsp). We believe this will serve as a useful tool for researchers in the field of skeletal development.

H. Isshiki · K. Sato (✉) · K. Horiuchi · H. Ikegami · Y. Toyama
Department of Orthopedic Surgery, School of Medicine, Keio University, 35 Shinanomachi, Shinjuku-ku, Tokyo 160-8582, Japan
e-mail: kazuki@sc.itc.keio.ac.jp

S. Tsutsumi · H. Aburatani
Genome Science Division, Research Center for Advanced Science and Technology, The University of Tokyo, Tokyo, Japan

M. Kano
Intelligent Cooperative System, Department of Information Systems, Research Center for Advanced Science and Technology, The University of Tokyo, Tokyo, Japan

H. Abe
Department of Pathology, School of Medicine, Keio University, Tokyo, Japan

A. Umezawa
Department of Reproductive Biology, National Research Institute for Child Health and Development, Tokyo, Japan

Results and discussion

Two 9-day-old male ICR mice were used for the analysis. The tibiae were harvested, embedded in OCT, and immediately frozen in liquid nitrogen. Forty cryosections 10 μm thick were prepared, and the tissues from each growth plate zone were identified and collected using a laser microdissection microscope (Fig. 1a). All animal experiments were approved by the Institutional Animal Care and Use Committee of the School of Medicine, Keio University. The samples from each individual mouse (#1 and #2) were analyzed separately. The gene expression profiles in the collected samples were analyzed using the GeneChip Mouse Genome 430 2.0 Array and Affymetrix Microarray Suite v5.0 (Affymetrix). Approximately 14,500 transcripts (out of 45,101 probes on the chip) whose signal intensity was above the detection level, were further filtered to eliminate those transcripts expressed at a very low level, or those hybridized to a non-functional probe. Finally, 2,427

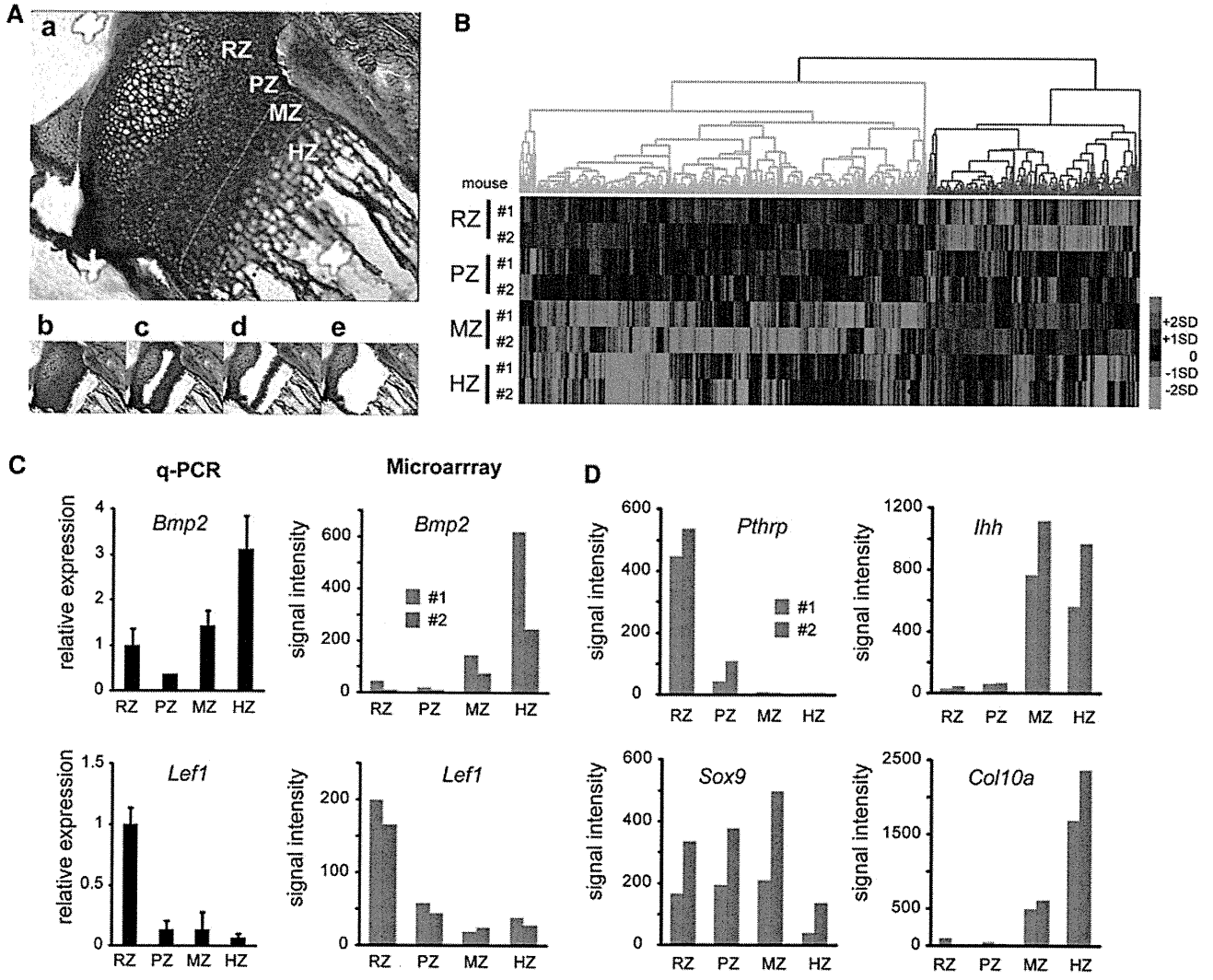

Fig. 1 **a** Representative photomicrographs for the laser microdissection procedure. *a* Sagittal cryosection of the tibia stained with Giemsa. Areas circumscribed by *broken lines* represent each zone of the growth plate. Tissue from these sections was sequentially harvested from the HZ (*b*), RZ (*c*), PZ (*d*), and MZ (*e*). **b** Hierarchical clustering dendrogram and heat map showing 1,955 genes expressed in the growth plate. Gene expression profiles of two individual mice (#1 and #2) are presented. Relatively tight clustering was seen in the genes expressed in the RZ and PZ (*yellow*), and in the MZ and HZ (*blue*). **c** Expression patterns of the transcripts for *Bmp2* and *Lef1* evaluated by qPCR and microarray analysis. Gene expression levels of the two individual mice (#1 and #2) deduced from the microarray analysis are presented. **d** Expression profiles of *Pthrp*, *Ihh*, *type 10 collagen* (*Col10a*), and *Sox9* in the two individual mice (#1 and #2) deduced from the microarray analysis

transcripts, corresponding to 1,995 different genes, were identified. Detailed description of the procedures, including RNA extraction, cRNA probe labeling, gene chip hybridization, and data analysis, will be provided on request.

To obtain an overview of the gene expression profiles, we first performed hierarchical clustering analysis of the transcripts expressed in each zone of the growth plates from two individual mice. As shown in Fig. 1b, it was clear from this analysis that the gene expression profiles of each growth plate zone were highly reproducible between the individual mice. Interestingly, we found that the dendrogram divided into two main branches: the gene clusters expressed in the early stage of differentiation of chondroblasts (RZ and PZ), and those expressed in the later stage (MZ and HZ) (Fig. 1b), indicating that chondroblasts undergo drastic changes in their gene expression profile during their transition from PZ to MZ.

To confirm that the RNA amplification and data processing did not skew the actual expression patterns of the transcripts in vivo, we compared the expression levels of several genes deduced from the microarray analysis with those evaluated by quantitative PCR (qPCR). As illustrated by the examples shown in Fig. 1c, *Bmp2* (which is predominantly expressed in the HZ) and *Lef1* (a transcriptional mediator of Wnt/β-catenin signaling), we found a significant correlation in the expression patterns of all the

genes we examined, suggesting that the gene expression levels deduced from the microarray analysis in this study were comparable with those measured by qPCR.

We next examined the expression patterns of several genes whose functions and expression patterns in the growth plate have been well characterized, to evaluate whether our data could reproduce previous findings. For example, the feedback loop between *Pthrp* and *Ihh* in the growth plate plays an essential role in longitudinal skeletal growth [2], and the expression of these genes is known to be mutually exclusive in vivo; the transcripts for *Pthrp* are found in the RZ, and those for *Ihh* in the HZ. As shown in Fig. 1d, our data sets clearly reproduced this observation. Furthermore, the expression profiles of *type 10 collagen* (which is specifically expressed in the HZ) and *Sox9* (which is induced in the RZ, PZ, and MZ, but not in the HZ), were also consistent with past studies [3]. Taken together, these findings indicate that our sampling of tissue from each growth plate zone was accurate, and that the expression profiles deduced from microarray analysis reflected the actual expression patterns of a given gene in vivo, with high reproducibility.

Because of the difficulty of obtaining tissue from each of the specific zones of the murine growth plate in terms of both quantity and quality, it has been difficult to perform comprehensive analysis of the expression profiles of genes in the growth plate. Here, using a combination of laser microdissection and microarray analysis, we have successfully established a data set that contains the expression profiles of 1,995 different genes expressed in the growth plate. Although similar studies have been reported [4–6], our study is unique in three respects:

1. the data were obtained by use of a mouse genome expression array containing 45,100 probes and approximately 34,000 genes, which enabled the most comprehensive analysis of genome-wide expression currently available;
2. by using a laser microdissection microscope, cartilage tissue was collected from the four distinct zones in the growth plate with high accuracy, enabling precise spatial analysis of the gene expression patterns; and
3. the data set was made publicly available for investigators via an on-line database.

The mechanisms governing the differentiation of chondroblasts in the growth plate are very complex, and many of the molecular mechanisms behind skeletal development remain to be elucidated. We believe that the gene expression data established in this study will facilitate further investigation in this field.

Conflict of interest The authors declare no conflict of interest.

References

1. Karsenty G, Wagner EF. Reaching a genetic and molecular understanding of skeletal development. Dev Cell. 2002;2:389–406.
2. Kronenberg HM. Developmental regulation of the growth plate. Nature. 2003;423:332–6.
3. Adams SL, Cohen AJ, Lassova L. Integration of signaling pathways regulating chondrocyte differentiation during endochondral bone formation. J Cell Physiol. 2007;213:635–41.
4. Belluoccio D, Bernardo BC, Rowley L, Bateman JF. A microarray approach for comparative expression profiling of the discrete maturation zones of mouse growth plate cartilage. Biochim Biophys Acta. 2008;1779:330–40.
5. Wang Y, Middleton F, Horton JA, Reichel L, Farnum CE, Damron TA. Microarray analysis of proliferative and hypertrophic growth plate zones identifies differentiation markers and signal pathways. Bone. 2004;35:1273–93.
6. Benoyahu D, Akavia UD, Socher R, Shur I. Gene expression in skeletal tissues: application of laser capture microdissection. J Microsc. 2005;220:1–8.

STEM CELLS®

STEM CELL TECHNOLOGY: EPIGENETICS, GENOMICS, PROTEOMICS, AND METABONOMICS

Treatment of Human Mesenchymal Stem Cells with Angiotensin Receptor Blocker Improved Efficiency of Cardiomyogenic Transdifferentiation and Improved Cardiac Function via Angiogenesis

YOHEI NUMASAWA,[a] TAKEHIRO KIMURA,[a] SHUNICHIRO MIYOSHI,[a] NOBUHIRO NISHIYAMA,[a] NAOKO HIDA,[a] HIROKO TSUJI,[a] HIKARU TSURUTA,[a] KAORU SEGAWA,[b] SATOSHI OGAWA,[a] AKIHIRO UMEZAWA[c]

[a]Department of Cardiology and [b]Department of Microbiology and Immunology, Keio University School of Medicine, Tokyo, Japan, [c]Department of Reproductive Biology and Pathology, National Research Institute for Child Health and Development, Tokyo, Japan

Key Words. Angiotensin • Bone marrow stromal cells • Transdifferentiation • Stem cell transplantation

ABSTRACT

To improve the modest efficacy of mesenchymal stem cell (MSC) transplantation, the treatment of human MSCs with angiotensin receptor blockers (ARBs) was investigated. MSCs were cultured with or without the medium containing 3 μmol/l of ARBs before cardiomyogenic induction. After cardiomyogenic induction in vitro, cardiomyogenic transdifferentiation efficiency (CTE) was calculated by immunocytochemistry using anticardiac troponin-I antibody. In the nude rat chronic myocardial infarction model, we injected MSCs pretreated with candesartan (A-BM; $n = 18$) or injected MSCs without pretreatment of candesartan (BM; $n = 25$), each having survived for 2 weeks. The left ventricular function, as measured by echocardiogram, was compared with cardiomyogenic transdifferentiation in vivo, as determined by immunohistochemistry. Pretreatment with ARBs significantly increased the CTE in vitro (10.1 ± 0.8 $n = 12$ vs. 4.6 ± 0.3% $n = 25$, $p < .05$). Transplantation of candesartan-pretreated MSCs significantly improved the change in left ventricular ejection fraction (BM; −7.2 ± 2.0 vs. A-BM; 3.3 ± 2.3%). Immunohistochemistry revealed significant improvement of cardiomyogenic transdifferentiation in A-BM in vivo (BM; 0 ± 0 vs. A-BM; 0.014 ± 0.006%). Transplantation of ARB-pretreated MSCs significantly improved cardiac function and can be a promising cardiac stem cell source from which to expect cardiomyogenesis. STEM CELLS *2011;29:1405–1414*

Disclosure of potential conflicts of interest is found at the end of this article.

INTRODUCTION

Regeneration therapies have attracted a great deal of medical attention. Various cellular resources such as embryonic stem cells [1], mesenchymal stem cells (MSCs) [2], mononuclear cells [3, 4], and endothelial progenitor cells (EPCs) [5] have been candidates for the regeneration therapies. The majority of cells derived from bone marrow (BM) consist of blood cells in various stages of differentiation; however, BM also contains, hematopoietic stem cells, EPCs, and MSCs. MSCs have characteristics of replication competence and multipotency [2, 6–8], as reported in numerous studies of MSCs.

Mesenchymal cells are classified as somatic stem cells and exist in BM stroma, dermis, skeletal muscle, uterine endometrial gland [9], umbilical cord blood [7, 10], placenta [11], amniotic membrane [6], etc. They are known to be capable of transdifferentiating into bone, cartilage, skeletal muscles, fats, ligaments, vascular endothelium, smooth muscle, and cardiomyocytes. Among the various mesenchymal cell sources, BM-derived MSCs (BM-MSCs) can be used in an autologous manner; therefore, there are no immunological problems in transplantations. However, in terms of cardiomyogenic transdifferentiation, the efficiency of human BM-MSCs is extremely low [8] in vitro, and efficiency of human BM-MSC transplantation is modest in in vivo [12, 13] and in clinical trials [14, 15]. The limited effect in clinical trials may be due to low angiogenic and paracrine effect of human BM-MSCs, low cardioprotective effect on host myocardium, and partially due to low cardiomyogenic transdifferentiation efficiency (CTE) [8]. We have previously shown that human mesenchymal cells derived from younger populations, that is,

Author contributions: Y.N., T.K., N.N., H. Tsuji, H. Tsuruta, and K.S.: conception and design, collection and assembly of data, final approval of manuscript; S.M.: conception and design, administrative support, collection and assembly of data, data analysis and interpretation, manuscript writing, final approval of manuscript; N.H.: conception and design, collection and assembly of data; S.O.: financial support, administrative support, final approval of manuscript; A.U.: financial support, administrative support, final approval of manuscript. Y.N. and T.K. contributed equally to this article.

Correspondence: Shunichiro Miyoshi, M.D., Ph.D., Keio University School of Medicine, 35-Shinanomachi, Shinjuku-ku, Tokyo 160-8582, Japan. Telephone: 81-3-3353-1211, ext. 61421; Fax: 81-3-5363-3875; e-mail: smiyoshi@cpnet.med.keio.ac.jp Received March 8, 2011; accepted for publication June 30, 2011; first published online in STEM CELLS *EXPRESS* July 13, 2011.
1066-5099/2009/$30.00/0 doi: 10.1002/stem.691

endometrial gland [9], umbilical cord blood [10], placenta [11], and amniotic membrane [6] have a high CTE and a beneficial effect on cardiac function. Therefore, we hypothesized that mesenchymal cells obtained from younger populations might have a better effect on regeneration therapies. As angiotensin receptor blocker (ARB) was known to have the potential to play a role in the anti-aging effect, we postulated that ARB might improve the efficacy of BM-MSCs on cardiac stem cell therapy.

Stimulation of angiotensin receptors is known to be related to adipogenic transdifferentiation of human BM-MSCs [16]. In the brain ischemic reperfusion model, BM-MSC transplantation significantly reduced the brain infarction area via improvement of brain blood flow and reduction of oxidative stress [17]. The effect of BM-MSC transplantation was abolished by knocking out the angiotensin-II (AT) receptor type-II (AT2R). On the other hand, this effect was restored by pretreatment with ARB for BM-MSCs in the culture. These facts suggest that ARB and stimulation of AT receptor may play a significant role in causing the angiogenesic effect of BM-MSC transplantation. Therefore, in this study, we investigated the effect of ARB on CTE of human BM-MSCs in vitro and in vivo, and efficacy of BM-MSC transplantation on cardiac function in the myocardial infarction (MI) model in vivo.

Materials and Methods

BM-Derived MSCs

Yub623 (RIKEN Cell bank, Cell No. HMS0017, Tokyo, Japan) cells were used as BM-MSCs in this study. Yub623 is a fibroblast-like shaped human MSC (hMSC) derived from neonatal human BM from a finger of patients with polydactyly. Cells were cultured in high-glucose supplemented Dulbecco's modified Eagle's medium containing 10% human serum.

Cardiomyogenic Induction and Chemical Agents

The method of cardiomyogenic induction in vitro was described previously (Supporting Information Material and Method-1) [6, 8–11]. In short, enhanced green fluorescent protein (EGFP) labeled BM-MSCs were cocultured with murine cardiomyocytes. In this system, the incidence of cell fusion was approximately 0.3% and the evidence of cell fusion-independent cardiomyogenesis was extensively shown in the previous studies [6, 8–11, 18, 19]. BM-MSCs were preincubated with chemical agent-containing medium for 2 weeks before coculture and/or cultured with chemical agent-containing medium after coculture. In this study, we used 3 μmol/l of telmisartan (tel), candesartan (cnd), losartan (los), olmesartan (olm), and valsartan (val) as an AT receptor blocker (ARB), 3 μmol/l of PD123319 (pd) as a specific AT type-I blocker; enalaprilat (ena) and captopril (cap) as an angiotensin converting enzyme (ACE) inhibitor; 3 μmol/l of aliskiren (ali) as a direct rennin inhibitor; 1 μmol/l of AT; and 10 μmol/l of GW9662 (gw) as a peroxisome proliferators-activated receptor-γ (PPAR-γ) blocker. Evaluation of efficiency of cardiomyogenic transdifferentiation was described previously [6, 10, 11]. In short, cocultivated BM-MSCs were enzymatically isolated, a smear sample was made, and then immunocytochemistry using mouse monoclonal antibody against anticardiac troponin-I (Trop-I, #4T21 Hytest, Euro, Finland) antibody was performed (described later). Isolated cells (spherical shape), in which Trop-I colocalized with EGFP at the cytoplasm were considered as Trop-I/EGFP double positive cells. The CTE was defined as the incidence of Trop-I/EGFP double positive cells in EGFP-positive BM-MSCs. The incidence of cell fusion was not affected by ARB treatment (0.30% to 0.39%) in this study.

Immunocytochemistry and Immunohistochemistry

A laser confocal microscope (FV1000, Olympus, Tokyo, Japan) was used. As described previously [6, 8–11, 18, 19], samples were stained with Trop-I with mouse monoclonal antibody (sigma) and rabbit polyclonal anti-connexin 43 antibody (sigma) diluted 1:300 overnight at 4°C, then stained with TRITC-conjugated anti-mouse IgG antibody (Sigma) and Cy5-conjugated anti-rabbit IgG antibody (Chemicon) diluted 1:100, containing 4′-6-diamidino-2-phenylindole (Wako) at 1:300 for 30 minutes at 25–28°C.

Enzyme-Linked Immunosorbent Assay

Angiogenic humoral factors (angiogenin, angiotensin-2, epidermal growth factor [EGF], basic fibroblast growth factor, heparin-binding EGF-like growth factor, hepatocyte growth factor, phosphatidylinositol-glycan biosynthesis class F protein, and vascular endothelial growth factor) in culture medium supernatant (cultured with 10% serum-containing medium for 7 days) were measured by enzyme-linked immunosorbent assay [19]. The assay was performed with Quantibody Human Angiogenesis Array I kit (RayBiotec, Inc. GA) and was conducted according to manufacturer recommended protocol.

Gene Chip Analysis

Human genome-wide gene expression was examined with the Human Genome U133A Probe array (Affymetrix), which contains the oligonucleotide probe set for approximately 23,000 full-length genes and expressed sequence tags as described previously [11, 20].

Transplantation of ARB-Pretreated BM-MSCs in MI Model In Vivo

MI was induced in the open chests of anesthetized female F344 nude rats (Clea Japan, Inc., 6 weeks of age) as described previously [6, 9, 19]. Two weeks after MI, 1–2 $\times$ 10^6 of EGFP-labeled BM-MSCs were injected into the myocardium at the border zone of the MI. Two weeks after the first operation, rats with MI were randomized in a blind study of the following groups: the sham operated group (Sham), the (CNT), the CNT with plain BM-MSC transplanted group (BM), and the MI+candesartan-pretreated BM-MSC transplanted group (A-BM). After cellular transplantation, TCV-116 (stable form of candesartan; 0.5 mg/kg/day) was orally administered in some of the experiments (+A). Randomization occurred immediately before echocardiogram. Immediately before cell transplantation, two-dimensional and M-mode echocardiographic (8.5 MHz linear transducer; EnVisor C, Phillips Medical System, Andover, MA) images were obtained to assess left ventricular (LV) end-diastolic dimension and LV end-systolic dimension (LVESD) at the mid-papillary muscle level by a single blinded observer. Two weeks after the transplantation, a similar echocardiogram was performed again. LV percentage fractional shortening, thickness of anterior wall (AW), and thickness of posterior wall were calculated from five to six traces and averaged. LV pressure, brain natriuretic peptide (BNP), body weight, and heart weight (wet) were measured as described previously. Tissue samples were obtained by slicing along the short axis of the left ventricle, for every 1 mm of depth. After masson trichrom staining, the area of fibrosis was digitized from each slice, and then the percentage fibrosis volume in the LV myocardium was calculated as described previously [6, 19]. Immunohistochemical analysis was performed to observe CTE in vivo as described previously (Supporting Information Material and Method-2). Immunohistochemical analysis was performed using anti-rat CD34 antibody (1:200 R&D Systems; AF4117) to evaluate vascular density. Then, biotinylated goat immunoglobulins (Dako; E0466) were used as a second antibody, next, strept avidin biotin complex (ABC) complex/horseradish peroxidase (HRP) (Dako; K0377), and, finally, 3,3′-Diaminobenzidine substrate (Wako; K3183500) were used. The images were digitized and the percentage brown pixel area of the capillary vessels was counted in the peri-infarct normal zone (NZ) and the center of the MI

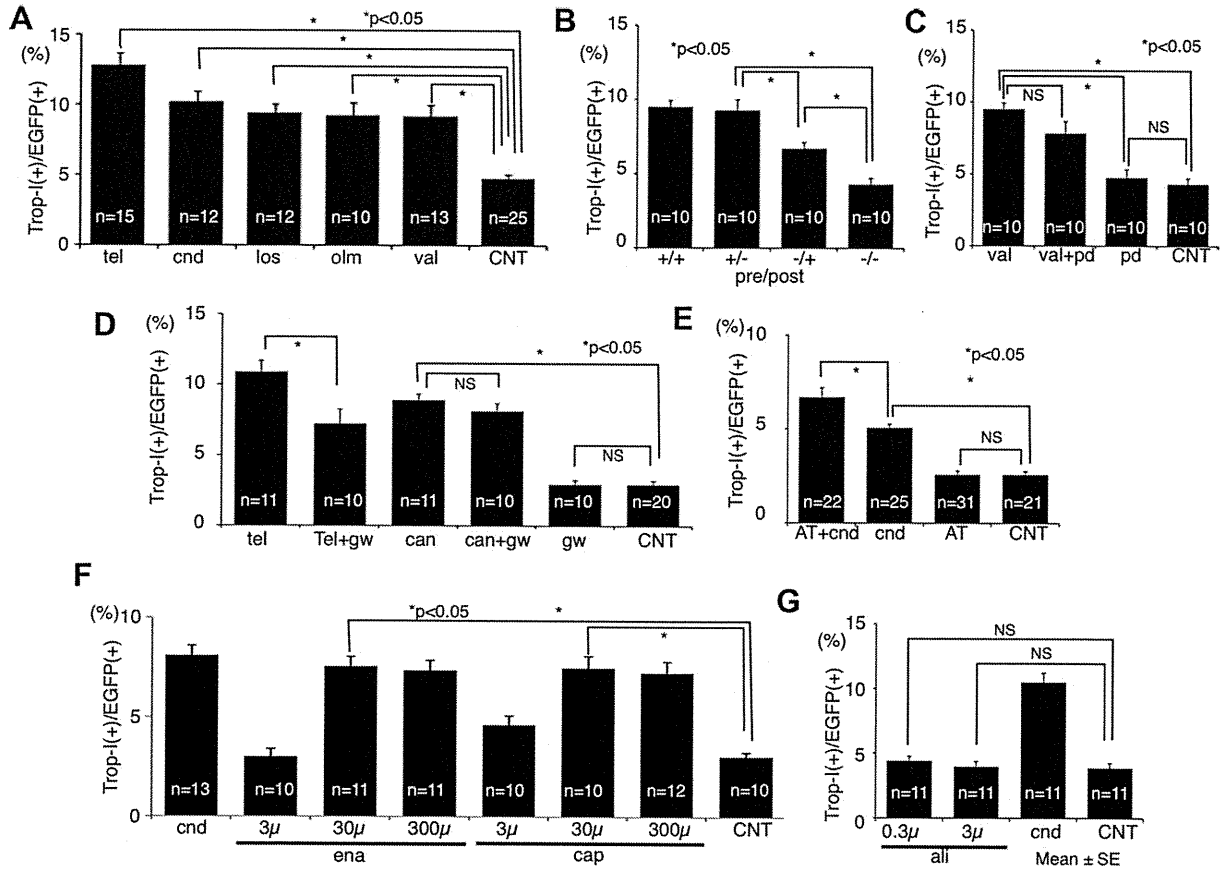

Figure 1. Improvement of cardiomyogenic transdifferentiation efficiency (CTE) of bone marrow-derived mesenchymal stem cells (BM-MSC) by blockade of renin-angiotensin system in vitro. The calculated rate of cardiac troponin-I positive cells in enhanced green fluorescent protein-positive cells are averaged and shown as CTE. **(A):** The effect of pretreatment with telmisartan (tel), candesartan (cnd), losartan (los), olmesartan (olm), and valsartan (val) on CTE of human BM-MSCs are shown. CNT denoted CTE of control MSCs. These ARBs increase CTE significantly. **(B):** Condition of pretreatment of val (before slash) and val treatment after induction (after slash) are shown in the bottom. Pretreatment of val significantly increased CTE and was essential for val-induced CTE increase. Val treatment after induction moderately increased CTE. **(C):** The effect of combination of val as a specific angiotensin-II (AT) receptor type-I (AT1R) blocker and PD123319 (pd) as a specific AT2R blocker to CTE is shown. The pd did not affect CTE. **(D):** The effect of GW9662 (gw) as a specific peroxisome proliferators-activated receptor-γ (PPAR-γ) blocker on tel-induced CTE increase and cnd-induced CTE increase are shown. The blockade of PPAR-γ partially blocked the tel-induced CTE increase and did not affect cnd-induced CTE increase. **(E):** The effect of additional application AT in the presence or in the absence of cnd is shown. AT alone did not affect CTE; however, AT significantly increased CTE in the presence of cnd. **(F):** Dose-response effect of pretreatment with enalaprilat (ena) and captoril (cap) as angiotensin converting enzyme inhibitors (ACEI). ACEI significantly improves CTE in a dose-dependent manner. **(G):** The effect of aliskiren (ali) as a renin inhibitor on CTE is shown. Ali did not affect CTE. *p<0.05. Abbreviations: ali, aliskiren; AT, angiotensin-II; cap, captoril; cnd, candesartan; CNT, control; EGFP, enhanced green fluorescent protein; ena, enalaprilat; gw, GW9662; los, losartan; olm, olmesartan; pd, PD123319; Tel, telmisartan; Trop-I, troponin-I; val, valsartan.

zone (MI) using a light microscope at 10× magnification. The areas in five high-power fields were calculated and averaged.

Statistical Analysis

All data are shown as mean value ± SE. The difference between mean values was determined with one-way analysis of variance (ANOVA) test or one-way repeated measures ANOVA test and Bonferroni post hoc test. Statistical significance was set at $p < .05$.

Results

Pretreatment with ARB Increased Efficiency of Cardiomyogenic Transdifferentiation Via AT2R

Administration of 3 μmol/l of popular ARBs (tel, can, los, olm, and val) did not cause any significant change in morphology of BM-MSCs (Supporting Information Fig. 1A, 1B), while improved CTE in vitro was observed (Fig. 1A and Supporting Information Fig. 1C–1P). In our pilot study, we tested dose-response effect of ARBs and confirmed that this effect was saturated at the concentration of 3 μmol/l (CTE at control, 0.03, 0.3, 3, and 30 μmol/l of cnd were 3.0 ± 0.3, 3.5 ± 0.2, 4.8 ± 0.3, 8.9 ± 0.4, and 8.1 ± 0.5%, respectively). Therefore, in this study, we selected 3 μmol/l as a default concentration of ARBs. To clarify the target of the ARBs, val was administrated only before the coculture or only after the coculture (Fig. 1B). Administration of val after the start of coculture (±) caused modest improvement of CTE; on the other hand, administration of val before the start of coculture (±) significantly increased CTE, suggesting that val modified the character of the BM-MSCs so as to be able to cause higher CTE. To determine whether the effect of the ARBs was mediated by AT receptor type-I (AT1R) or AT2R, we used val as AT1R specific blocker and pd as AT2R specific blocker (Fig. 1C). Administration of pd did not affect CTE, while val increased CTE significantly. Furthermore, CTE with both val and pd administered did not show an additional increase

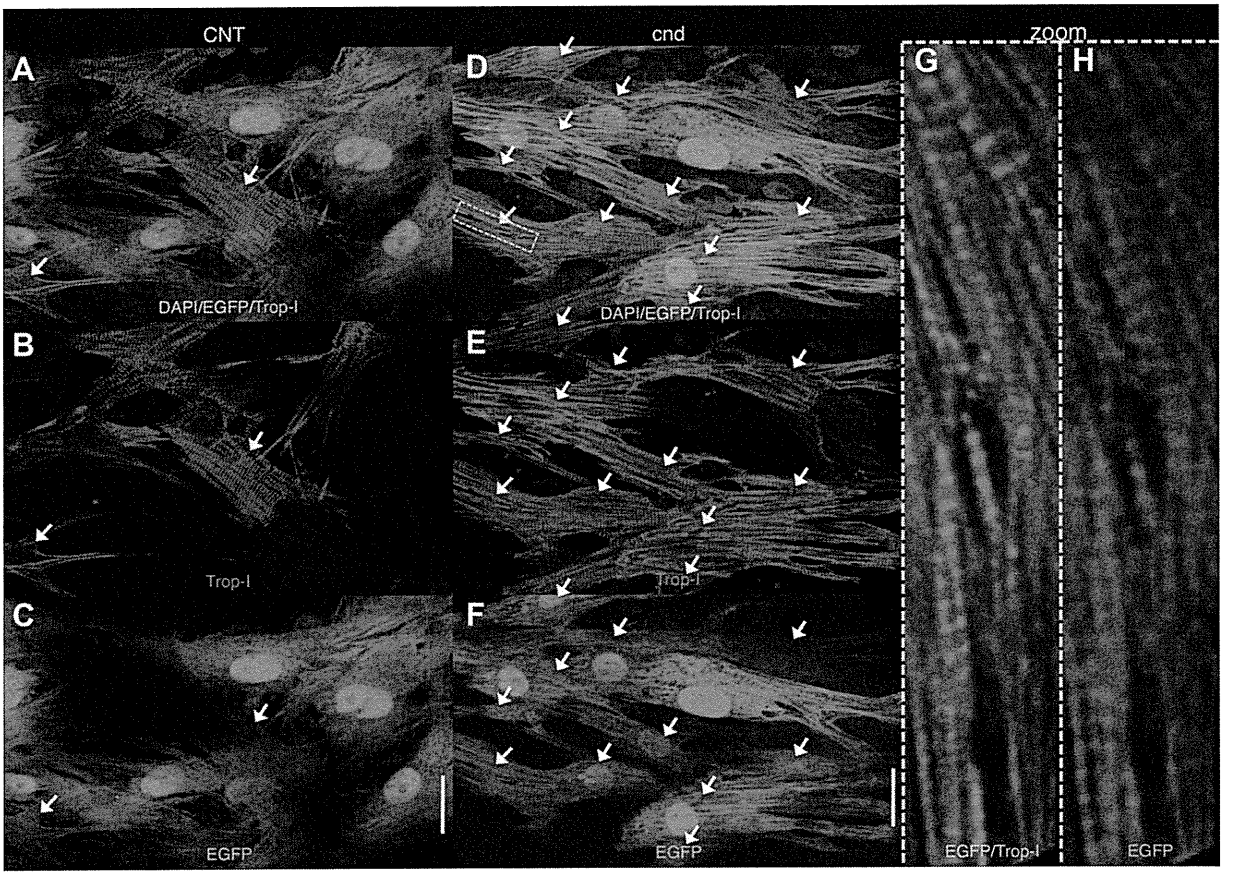

Figure 2. Confocal laser microscopic images of the immunocytochemical analysis of transdifferentiated cardiomyocytes. Confocal microscopic images of immunocytochemistry after cardiomyogenic induction using anti-cardiac troponin-I (red: Trop-I) revealed significant augmentation of enhanced green fluorescent protein (EGFP) (green)/Trop-I double positive cardiomyocytes (white arrow) by candesartan (cnd) (**D–F**) pretreatment, while EGFP/Trop-I double positive cells were rare in CNT (**A–C**). Area within the dotted yellow box is expanded and shown in (**G, H**). Clear striation staining pattern of Trop-I was observed in every EGFP-positive cell. The striating pattern of EGFP and Trop-I appeared in alternation, suggesting that the Trop-I was expressed in the EGFP-positive cells. Scale bar = 20 μm. Abbreviations: cnd, candesartan; CNT, control; DAPI, 4′-6-diamidino-2-phenylindole; EGFP, enhanced green fluorescent protein; Trop-I, troponin-I.

(rather, tended to show a statistically nonsignificant decrease). These data suggest that blockade of AT1R plays a pivotal role in ARB-dependent CTE increase. We have previously reported that PPAR-γ activator has an ability to increase CTE of BM-MSCs [19], and some of the ARBs, that is, tel, have a potential to activate the PPAR-γ. To clarify that the mechanism of ARB-induced CTE increase was mediated via PPAR-γ activation effect, we used gw as a specific blocker for PPAR-γ (Fig. 1D). The gw partially blocked tel-induced CTE increase; on the other hand, it did not block cnd-induced CTE increase. These data suggest that the effect of cnd on CTE was independent from PPAR-γ activation. In our previous study, the effect of pio was completely blocked by gw [19]; therefore, the gw-insensitive tel-induced CTE increase was caused by a PPAR-γ-independent mechanism. On the other hand, administration of AT did not affect CTE in the absence of ARB, while administration of AT significantly increased CTE in the presence of ARB (Fig. 1E). These data suggest both blockade of AT1R and stimulation of AT2R increase CTE. The increase in CTE was also observed by administration of ACE inhibitors ena or cap (Fig. 1F), suggesting the source of AT in this system is autocrine of angiotensin-I from BM-MSCs and local ACE activity. Furthermore, the effect was not blocked by the specific renin blocker, ali (Fig. 1G); therefore, angiotensinogen does not play a role as an AT source in this system, but a local angiotensin-generating system may play a role in this phenomenon.

The Effect of ARB-Treated BM-MSC Transplantation on Cardiac Function In Vivo

The BM-MSCs were transplanted into the hearts of nude rats with chronic MI, in vivo, and the effect on cardiac function was examined. Representative M-mode echocardiographic images at 2 weeks after transplantation are shown (Fig. 2A). In the CNT group, akinesis and thinning of AW are observed. There were no marked changes in the BM group, while in A-BM group, the motion of AW markedly improved. The same trend was also observed in the ARB orally administered group (+A group). The changes in echocardiographic parameters between the immediately before the transplantation group (post MI 2 weeks) and the 2 weeks after transplantation group (post MI 4 weeks) are compared (Fig. 3). Changes in LV ejection fraction (ΔLVEF) were decreased as a function of time, even 2 weeks after the MI, which may be due to LV remodeling. The transplantation of plain BM-MSCs (BM) did not have an effect on ΔLVEF; on the other hand, candesartan-pretreated BM-MSCs (A-BM) significantly improved ΔLVEF. The degree of improvement was marked when candesartan was orally administered (A-BM-A). Change in end-diastolic diameter of LV (ΔLVEDD) did not differ among the

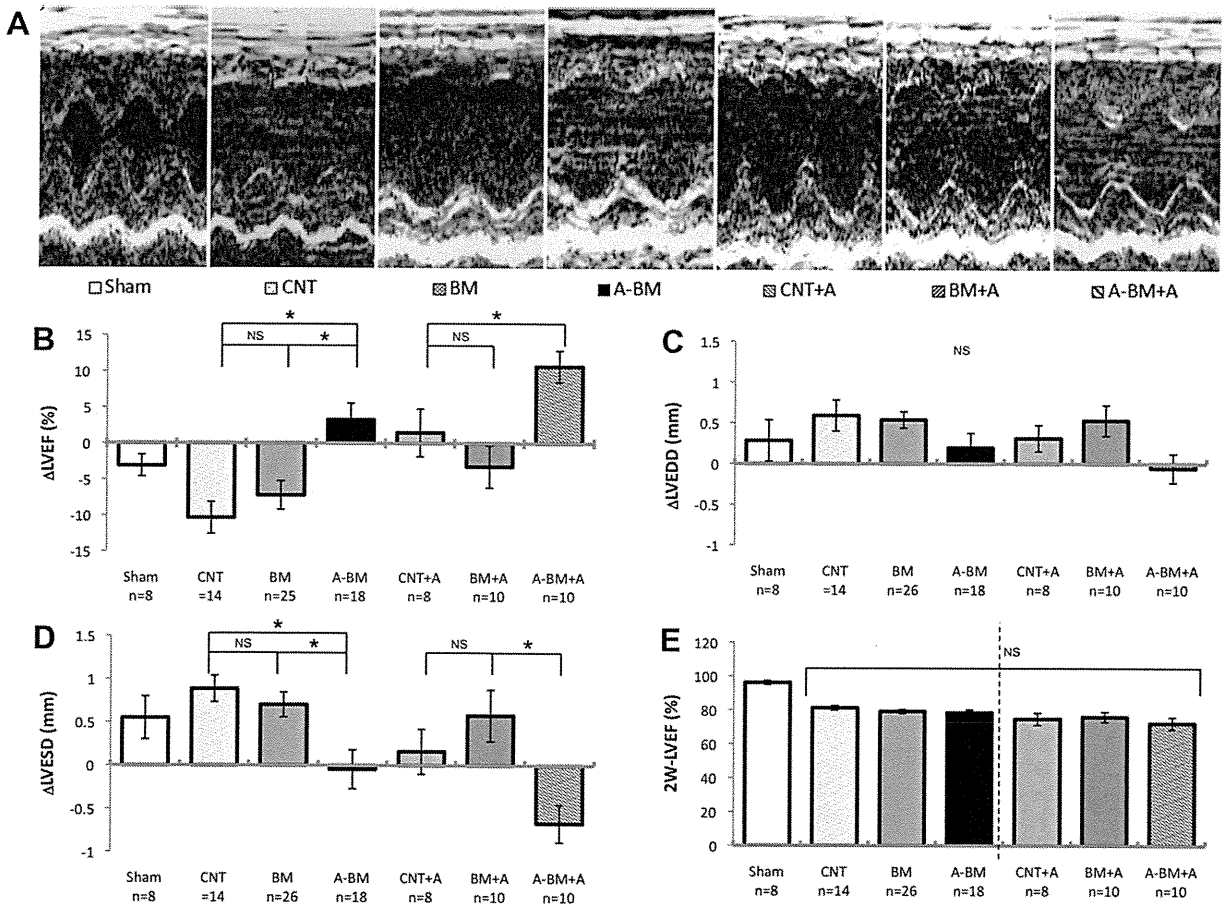

Figure 3. Effect of candesartan-pretreated bone marrow-derived mesenchymal stem cell (BM-MSC) transplantation and/or oral administration of candesartan on echocardiographic parameters in vivo. **(A):** Representative trace of M-mode echocardiogram from Sham-operated nude rats, control myocardial infarction (MI) (CNT), MI with BM-MSCs transplantation (BM), candesartan-pretreated BM (A-BM), and oral administration of candesartan after the transplantation (CNT+A, BM+A, A-BM+A) is shown. Changes in left ventricular ejection fraction (LVEF) from 2 to 4 weeks (**B**; ΔLVEF), LV end-diastolic dimension (**C**; ΔLVEDD), and LV end-systolic dimension (**D**; ΔLVESD) are averaged and shown. **(E):** Calculated LVEF from each group at 2 weeks after first operation are shown. There was no statistical significance; however, the degree of percentage EF tends to be worse in the oral administration series (right columns separated by dotted bar). Candesartan-pretreated BM significantly improved LVESD, consequently improved LVEF. *$p<0.05$. Abbreviations: BM, bone marrow; CNT, control; LVEDD, left ventricular end-diastolic dimension; LVEF, left ventricular ejection fraction; LVESD, left ventricular end-systolic dimension.

groups; on the other hand, change in LVESD (ΔLVESD) was significantly improved in A-BM group (vs. BM group) and A-BM+A group (vs. BM+A group), suggesting transplantation of candesartan-pretreated BM-MSCs significantly improved systolic function. Other echocardiographic parameter did not differ among the groups. There was no difference in the changes in body weight, serum BNP concentration, heart weight, LV systolic pressure, or LV end-diastolic pressure among the groups (Fig. 4). LV dP/dt was significantly improved by candesartan-pretreatment (A-BM vs. BM) with BM-MSCs; however, there was no additional effect of candesartan-pretreatment in the group of candesartan oral administration group (N.S. CNT-A vs. A-BM+A).

In this study, the beneficial effect was observed even in the ARB-pretreated BM-MSC transplantation group. The effect of ARB is known to cause an irreversible biological change in the cell, the "so-called" memory effect; therefore, such memory effect might affect cardiac function in vivo. To check this possibility, we cultured three groups of BM-MSCs: cells with candesartan for 2 weeks (ARB), cells without candesartan (CNT), and cells with candesartan for 1 week followed by 1 week without candesartan (1 week-ARB: washout for 1 week). The GeneChip analysis was performed among them, then the hierarchical clustering was used using the average distance method [20]. The gene expression pattern of 1 week-ARB was similar to CNT; therefore, the effect of ARB on BM-MSCs was reversible from the aspect of gene-chip analysis.

Incidence of Myocardial Transdifferentiation of ARB-Pretreated BM-MSCs In Vivo

To evaluate myocardial transdifferentiation of BM-MSCs in vivo, immunohistochemical analysis was performed. Antibodies against cardiac troponin-I (Trop-I) and connexin 43 were used. Confocal laser microscopic images could not detect EGFP-positive cardiomyocytes having clear striation staining pattern of Trop-I in the BM group. Sometimes enucleated EGFP-positive fragments of the cell at the center of the MI zone were observed, but taking the number of the injected EGFP-positive cells into account, the incidence seemed to be rare, as was reported previously [6, 19]. On the other hand, EGFP-positive and Trop-I double positive cells with clear striation staining pattern were observed at the marginal zone of the MI area in the candesartan-pretreated BM-MSC transplanted group (A-BM, Fig. 5F–5I). The oral

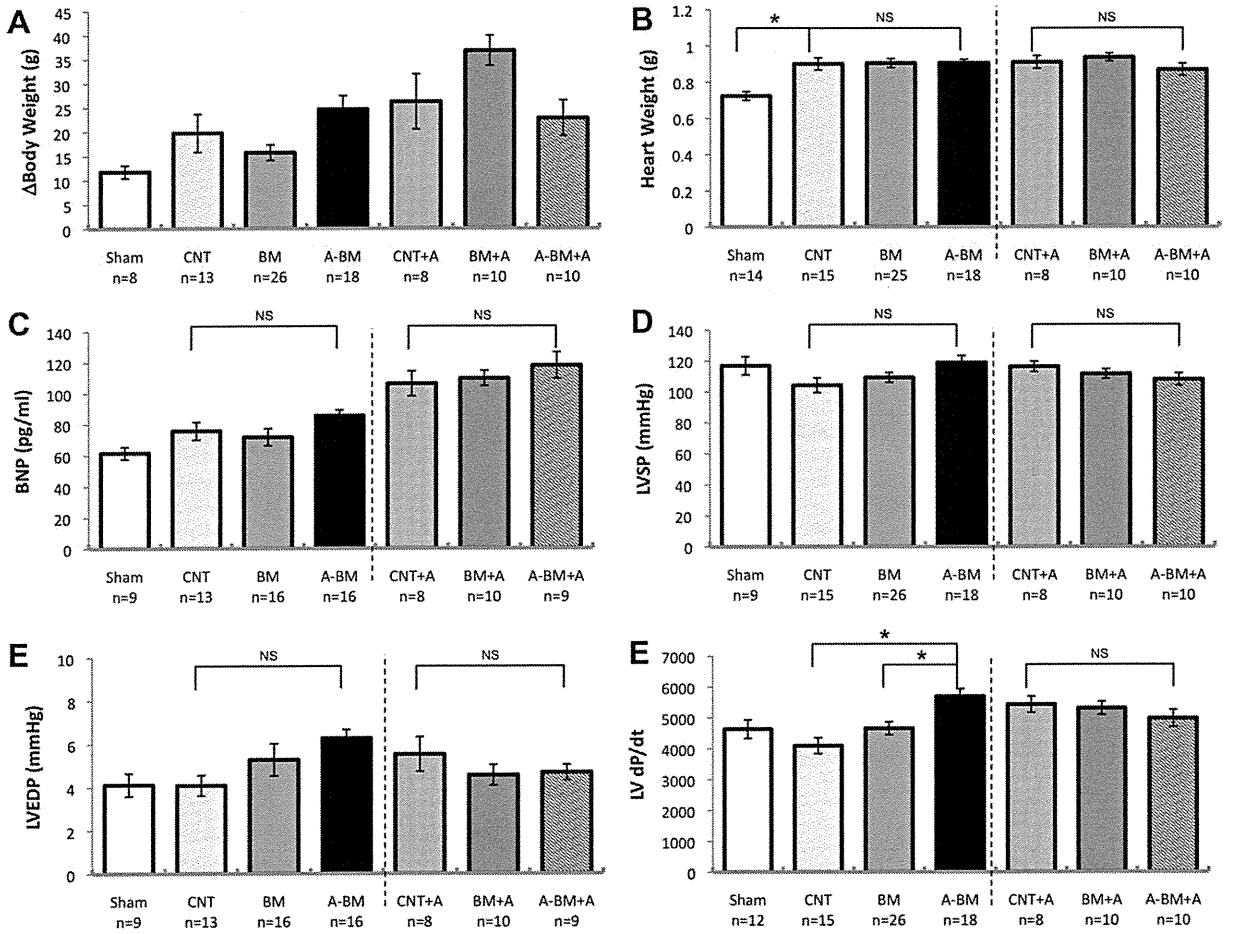

Figure 4. Effect of candesartan-pretreated bone marrow-derived mesenchymal stem cell (BM-MSC) transplantation and/or oral administration of candesartan on body weight, serum BNP concentration, and hemodynamic parameters. There was no difference in **(A)** changes in body weight, **(B)** heart weight, **(C)** BNP concentration, **(D)** left ventricular (LV) end-systolic pressure, or **(E)** end-diastolic pressure. **(D):** Effect of BM-MSCs on LV positive dP/dt is significantly improved by pretreatment with pioglitazone. **(F):** The LV dP/dt was significantly improved by transplantation of candesartan-pretreated BM-MSC (A-BM). *$p<0.05$. Abbreviations: BM, bone marrow; BNP, brain natriuretic peptide; CNT, control MI; LV, left ventricle; LVEDP, left ventricular end- pressure; LVSP, left ventricular systolic pressure.

administration of candesartan increased the incidence of survival of the EGFP/Trop-I double positive cells in vivo (A-BM+A, Fig. 5A–5E, 5J).

Genesis of Angiogenic Humoral Factors Derived from BM-MSCs by ARB

Angiogenic humoral factors were detected in the supernatant of the culture medium of BM-MSCs, suggesting that they are secreted from BM-MSCs, as reported previously [19]. However, the administration of 3 μmol/l of candesartan did not significantly affect the concentration of these angiogenic factors (Fig. 6). On the other hand, the angiogenic effect of candesartan-pretreated BM-MSCs was observed in vivo (Fig. 7A, 7B). In the peri-MI NZ, a CD34 positive area was not different among CNT, BM, and A-BM groups (without oral administration of candesartan). On the other hand, in the MI area, a CD34 positive area was significantly higher in A-BM group (vs. BM group). Oral administration of candesartan, significantly increased the CD34 area (CNT+A vs. CNT) in the peri-MI normal area and significantly increased it in the MI area. Masson trichrome staining and calculated MI volume at 2 weeks after transplantation (Fig. 7C, 7D) showed significant reduction of MI volume by pretreatment with candesartan of engrafted BM-MSCs (BM vs. A-BM) and the effect of pretreatment was not significantly augmented by the oral administration of candesartan.

Discussion

The Effect of Pretreatment with ARB in Human Neonatal BM-MSCs

The ARB did not affect the morphology of BM-MSCs and did not increase secretion of angiogenic humoral factors from BM-MSCs. The pretreatment with ARB significantly increased the CTE in vitro and in vivo. As pretreatment with ARB was essential for the effect on CTE, we concluded that the effect of ARB is not mediated by murine cultured myocardium, but directly affects BM-MSCs themselves, modifying the character of BM-MSCs. As the effect was not mediated by PD123319 as a selective AT2R blocker, the effect of ARB was mediated by the blockade of AT1R. In our previous article [19], activation of PPAR-γ significantly increased the CTE in BM-MSCs and the effect was completely blocked by GW9662, as a specific blocker of PPAR-γ receptor. The effect of telmisartan, which is known to have the strongest PPAR-γ activation activity among the ARBs, on CTE was partially blocked by GW9662, suggesting that the effect of ARBs is not mediated by PPAR-γ receptor activation activity. The

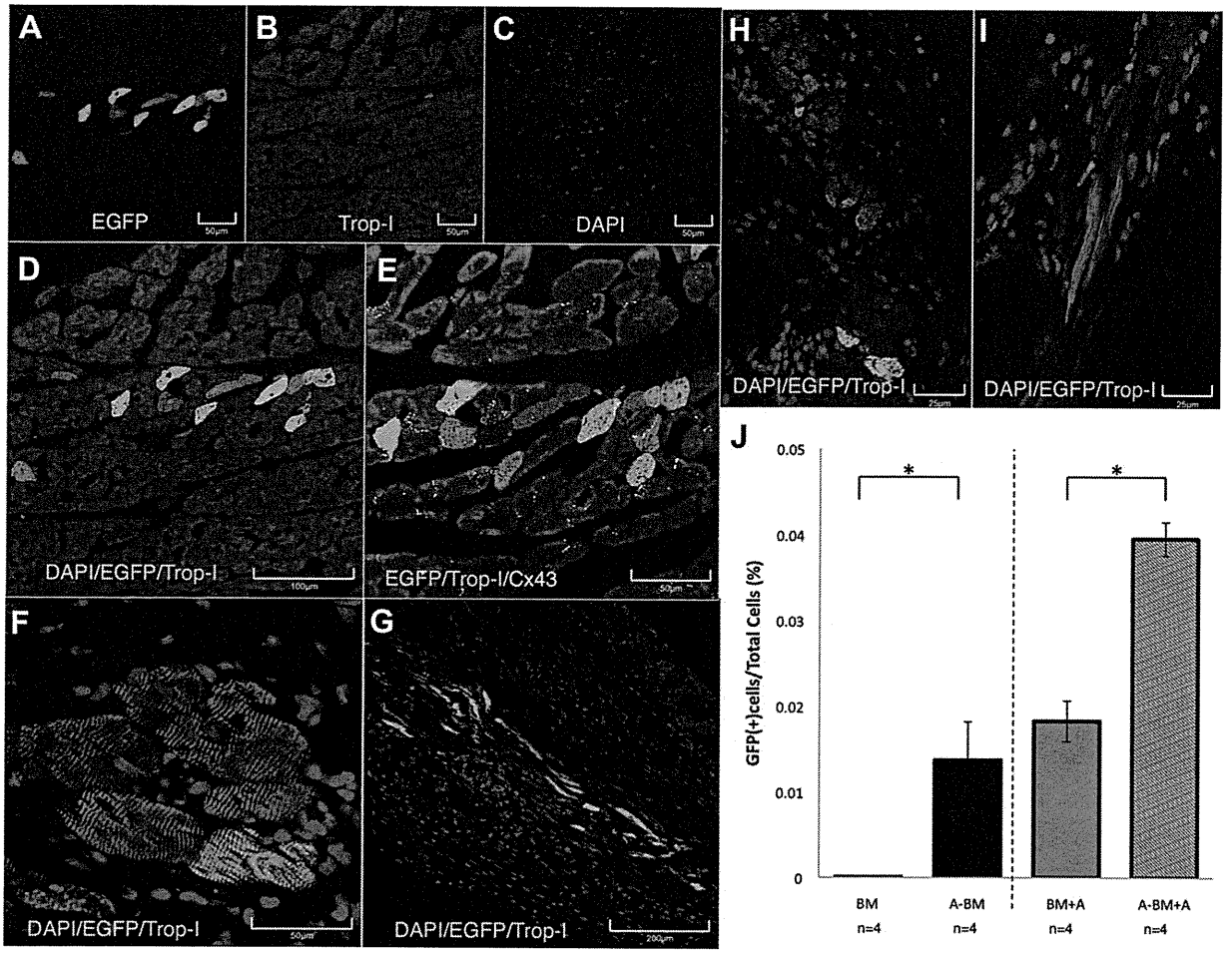

Figure 5. Both pretreatment and oral administration of candesartan significantly improved the incidence of survival of bone marrow-derived mesenchymal stem cell (BM-MSC)-derived cardiomyocytes in vivo. Confocal laser microscopic image of immunohistochemistry using anti-cardiac troponin-I antibody (red; Trop-I) is shown. **(A–C):** Lower magnification view for enhanced green fluorescent protein (EGFP) (green; **A**), Trop-I (**B**), and 4′-6-diamidino-2-phenylindole (Blue; **E**) is shown. After transplantation of candesartan-pretreated BM-MSCs in the presence of oral administration of candesartan (A-BM+A), EGFP-positive cells can be observed at the margin of the myocardial infarction (MI), but there were many EGFP/Trop-I double positive cardiomyocytes survived at the peri-MI zone **(A). (D):** Higher magnification view of merged image is shown. **(E):** The Trop-I positive cells are surrounded by dot-like staining of connexin 43 (white; Cx43). **(F):** Higher magnification view clearly shows striation staining pattern of Trop-I in the EGFP-positive cells. **(G):** At the center of MI zone (A-BM group), many EGFP-positive cells were enucleated and were negative for Trop-I. **(H, I):** However, there were some EGFP, Trop-I double positive rod-shaped cells at the center of MI zone. **(J):** The percentage of EGFP/Trop-I double positive cells in the injected EGFP-positive cells was averaged and is shown. By pretreatement with candesartan, the rate was significantly improved (A-BM vs. BM), and oral administration of candesartan additionally improved the incidence of EGFP/Trop-I double positive cells in vivo. Scale bars = 50 μm **(A–C, E, F)**, = 100 μm **(D)**, = 200 μm **(G)**, and = 25 μm **(H, I)**, respectively. *p<0.05. Abbreviations: BM, bone marrow; DAPI, 4′-6-diamidino-2-phenylindole; EGFP, enhanced green fluorescent protein; GFP, green fluorescent protein; Trop-I, troponin-I.

molecular mechanism of the effect of ARBs on CTE is still unclear. Further experiments should be done.

In the absence of valsartan as an AT1R selective blocker, administration of AT did not affect CTE; however, in the presence of valsartan, AT significantly increased CTE, suggesting that the relative stimulation of AT2R increased CTE. Furthermore, AT in culture medium seems to be generated by ACE activity in BM-MSCs, as the administration of ACE inhibitor to the BM-MSCs in culture significantly increased CTE in vitro. Furthermore, aliskiren did not affect the CTE; therefore, rennin and angiotensinogen did not play a role, but the angiotensin-I in the culture medium or autocrine from BM-MSCs must be a major source for AT.

Mechanism of Improving Systolic Function with ARB

Although EGFP-positive cardiomyocytes were observed in the candesartan-treated BM-MSC transplanted group, the number of them seems to be low for causing improvement in systolic function in vivo, as was seen in this study.

Concordant with the previous in vivo study [8] and clinical study [14], in the absence of BM-MSC transplantation, oral administration of candesartan suppressed the post-MI LV remodeling and progressive worsening of LVEF (CNT vs. CNT+A) at 2 weeks after MI. Furthermore, in this study, even in the absence of oral administration, the beneficial effect was observed in the candesartan-pretreated BM-MSC transplantation group. In this study, the effect of default BM-MSC transplantation was modest and there was no statistical significance from the control MI group. These data suggest that the ARBs modify the biology of BM-MSC, which play an important role in suppressing post-MI LV remodeling. This trend was observed in hemodynamic parameters and histological data. Pretreatment with candesartan significantly improved the efficacy of BM-MSC transplantation in augmentation of LV dP/dt and reduction in MI volume. Such

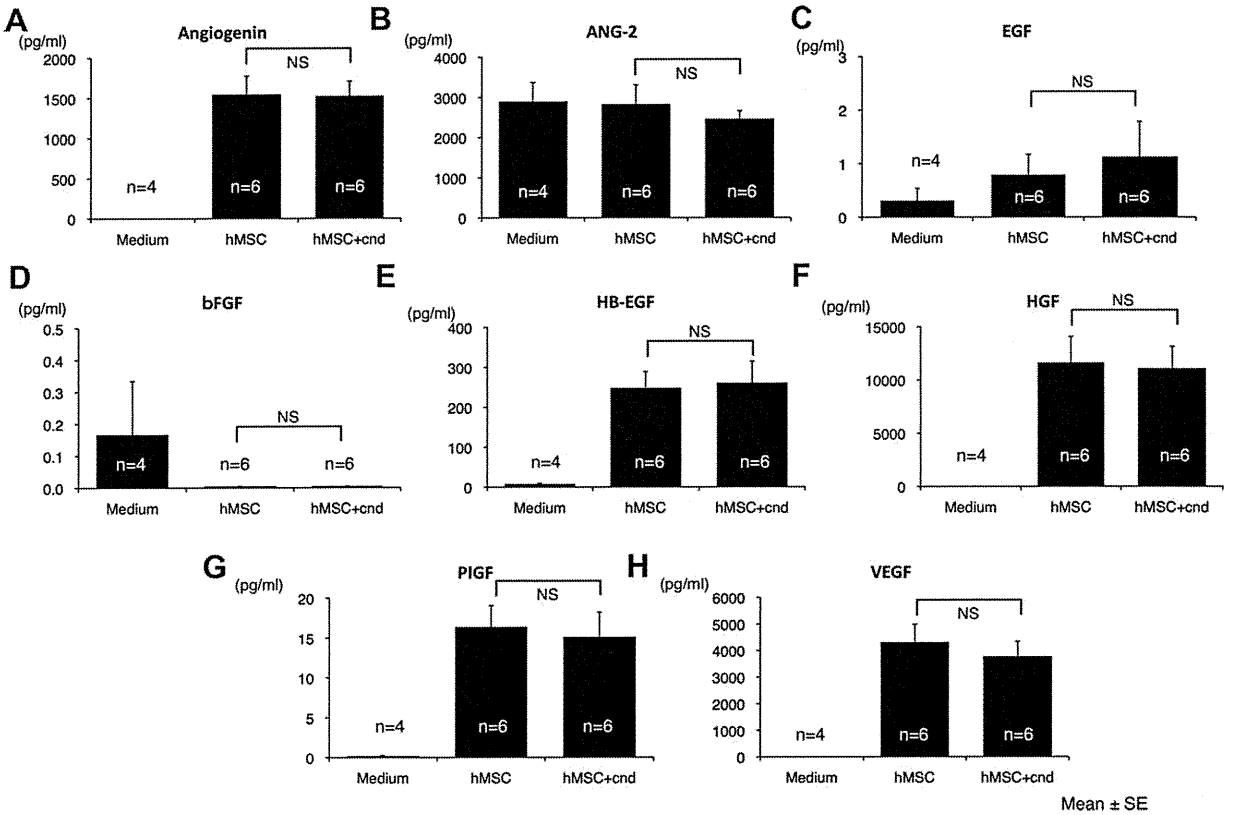

Figure 6. Secretion of angiogenic humoral factors from bone marrow-derived mesenchymal stem cells (BM-MSCs) into the culture medium supernatant and the effect of candesartan in vitro. Concentration of angiogenic humoral factors in **(A)** angiogenin, **(B)** angiotensin-2 (ANG-2), **(C)** epidermal growth factor (EGF), **(D)** basic fibroblast growth factor, **(E)** heparin-binding EGF-like growth factor, **(F)** hepatocyte growth factor, **(G)** phosphatidylinositol-glycan biosynthesis class F protein, and **(H)** vascular endothelial growth factor in culture medium was measured by enzyme-linked immunosorbent assay and averaged. Candesartan (cnd) treatment did not cause any significant change in angiogenic humoral factors secretion from BM-MSCs into the culture medium. Abbreviations: ANG-2, angiotensin-2; bFGF, basic fibroblast growth factor; cnd, candesartan; EGF, epidermal growth factor; HB-EGF, heparin-binding EGF-like growth factor; HGF, hepatocyte growth factor; hMSC, human mesenchymal stem cell; PIGF, phosphatidylinositol-glycan biosynthesis class F protein; VEGF, vascular endothelial growth factor.

cardioprotective effect of ARB-pretreated BM-MSCs may be due to augmentation of angiogenic effect and/or anti-apoptotic paracrine effect of BM-MSCs by pretreatment with ARB. The beneficial effect of ARB-pretreated BM-MSCs was also reported in the ischemia-reperfusion brain injury model [17], in which it was pointed out that both the stimulation of AT2R and blockade of AT1R have a significant effect on reducing brain damage in vivo and this data well correlated with our CTE data in vitro. In this study, the effect can be observed even by BM-MSC transplantation at 2 weeks after MI; therefore, the BM-MSC-induced angiogenesis might have suppressed ongoing post-MI LV remodeling. In this study, there was discrepancy between the angiogenic effect of ARB-pretreatment in BM-MSCs in vitro and in vivo. We speculated that additional angiogenic effect of BM-MSC transplantation by ARB-pretreatment might require graft-host interaction, that is, immunological reaction or inflammation in the host myocardium.

Cell Fusion-Independent Cardiomyogenic Transdifferentiation

Extensive evidence of cell fusion-independent cardiomyogenic transdifferentiation of human MSCs was presented in our previous study [6, 9–11, 19]. In this study, the incidence of cell fusion was approximately 1% and it was not affected by ARB pretreatment; therefore, the increase in EGFP-positive cardiomyocytes by ARB treatment was due to an increase in efficiency of cardiomyogenic transdifferentiation in vitro. Furthermore, there were no EGFP/Trop-I double positive rod shaped cardiomyocytes in the default BM-MSC transplanted group; on the other hand, the appearance of significant numbers of EGFP/Trop-I double positive cardiomyocytes was observed in ARB-pretreated BM-MSC transplanted group. This suggests an improvement of CTE of BM-MSCs in vivo by ARB pretreatment. Taking into account our previous study and our present in vitro experiment, we concluded that our observed EGFP/Trop-I double positive cells in vivo are caused by cardiomyogenic transdifferentiation.

Clinical Application

The efficacy of human BM-MSC transplantation had been modest [14, 15], and a new method for BM-MSC transplantation that will gain dramatic improvement in efficacy is expected. Genetic modification, that is, over-expression of the *AKT*-gene was reported to improve efficacy of BM-MSC transplantation in vivo [21]; however, use of such genetically modified cells raises a safety concern, that is, tumorgenecity. In comparison with the genetic modification, modification of BM-MSCs by ARBs, which are commonly used for heart failure patients, is a method that is ready to use for clinical patients.

In addition to the beneficial efficacy for cardiac function, this experimental model may also give us a clue to improving CTE in vivo, which is very essential for cardiac regenerative therapy. The precise mechanism for cardiomyogenic transdifferentiation of human BM-MSCs has been unclear. As the

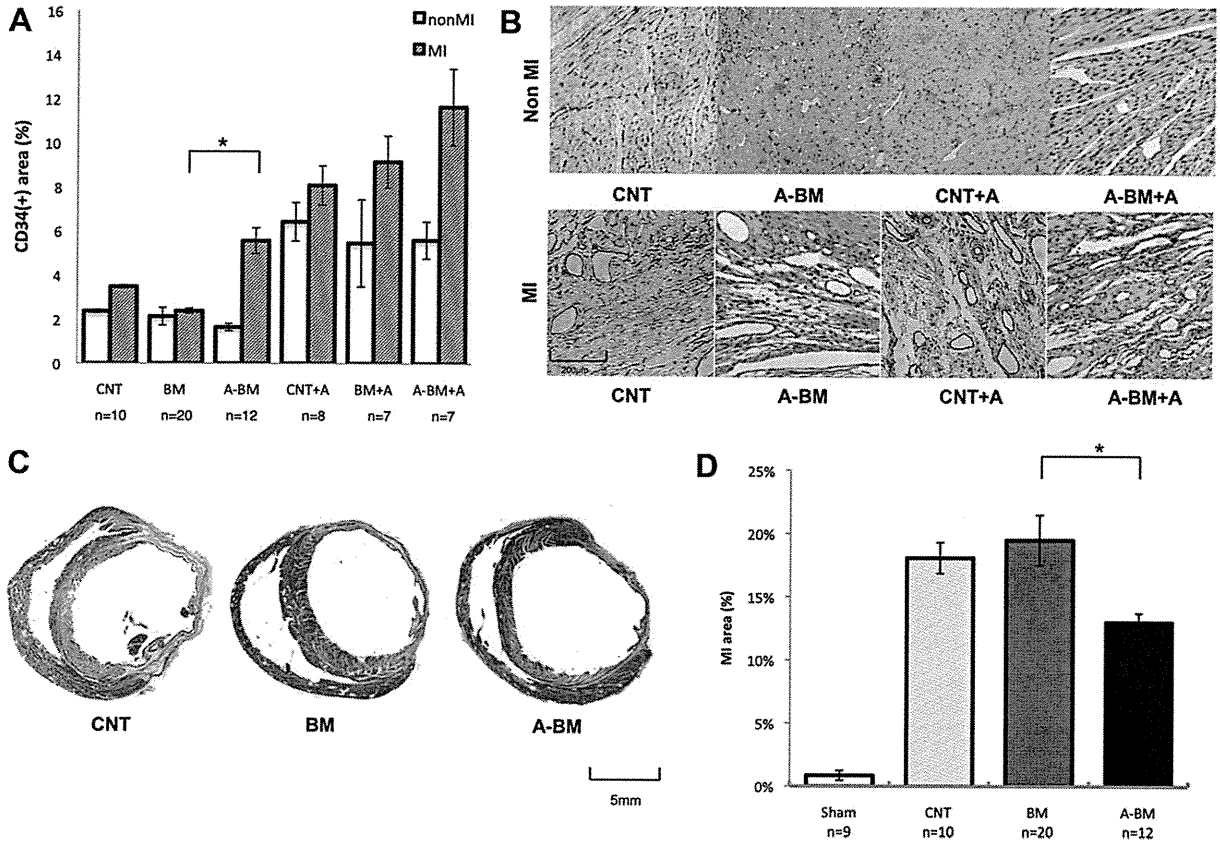

Figure 7. Effect of bone marrow-derived mesenchymal stem cell (BM-MSC) transplantation and/or treatment with candesartan on vessel density and infarction size in the heart in vivo. **(A):** The percentage of CD34 positive area in control myocardial infarction (MI) (CNT), MI with bone candesartan-pretreated BM-MSCs transplantation (BM), candesartan-pretreated BM (A-BM), and additional oral administration of candesartan after the transplantation (CNT+A, BM+A, A-BM+A) are calculated and averaged. **(B):** Representative microscopic image of immunohistochemistry using anti-CD34 antibody to detect vessels at center of MI zone and peri-MI normal zone (non-MI) are shown. Scale bar = 20 μm. Pretreatment with candesartan significantly increased vessel density at MI zone; on the other hand, oral administration of candesartan significantly increased vessel density at non-MI zone. **(C):** Representative masson-trichrom staining of the heart at the tendinous cord level of CNT, BM, and A-BM are shown. The digitized data were measured and calculated in **(D)**. By the candesartan-pretreatment, BM-MSC transplantation significantly decreased in percentage fibrosis volume. Scale bar = 5 mm. *p<0.05. Abbreviations: BM, bone marrow; CNT, control; MI, myocardial infarction.

incidence of cardiomyogenic transdifferentiation of human BM-MSCs is extremely rare, it has been impossible to statistically analyze the effect on CTE of various drugs or interventions in vivo. Therefore, there has been no systematic strategy for improvement of CTE of BM-MSCs until our previous article [6, 9–11, 19]. Our in vivo model of ARB-treated BM-MSCs is able to statistically analyze the effects of drugs on CTE, which is important for further improvement of CTE. In vitro, the pioglitazone's effect on CTE was independent from the effect of ARB; therefore, the additional administration of pioglitazone, as a PPAR-γ activator may be expected to improve CTE further. Further experiments should be done.

Study Limitation

In our previous study, we have used BM-MSCs obtained from a 41-year-old and a 90-year-old men. The CTE results were 1% and 0.3% in vitro [19], respectively. In this study, the CTE of default BM-MSCs from neonates was approximately 3%–5%. This data implies BM-MSCs obtained from younger generations that may have higher cardiomyogenic transdifferentiation ability. As ARB is known to have a potential for an anti-aging effect, the effect of ARB on BM-MSCs might increase the CTE by ARB's anti-aging effect on BM-MSCs. Further experiments should be done on this issue.

In vivo MI model was performed by two series (Sham, CNT, BM, A-BM series and CNT-A, BM-A, A-BM-A series) at different periods. As it was difficult to control the size of the MI at the coronary ligation, the size of the MI of later series are slightly larger (N.S.) than the former series. Therefore, we did not perform statistical analysis on some parameters between the series (separated by dotted line in the figures). The serum BNP level and the size of percentage MI volume are slightly larger in the later series. In this study, intra-individual difference values were compared with the values of the two series.

Conclusion

Pretreatment with angiotensin receptor blockers (ARBs) in culture activate human marrow-derived mesenchymal stem cells by angiotensin-II receptor type 1 blockade. ARBs-pretreated human marrow-derived msenchymal stem cells was significantly improved cardiomyogenic transdifferentiation efficiency in vitro and in vivo, and transplantation of the ARBs-pretreated cells significantly improved cardiac function and can be a promising cardiac stem cell source from which to expect cardiomyogenesis.

Acknowledgments

The research was partially supported by a grant from the Ministry of Education, Science and Culture, Japan. A part of this work was undertaken at the Keio Integrated Medical Research Center.

Disclosure of Potential Conflicts of Interest

The authors indicate no potential conflicts of interest.

References

1 Boheler KR, Czyz J, Tweedie D et al. Differentiation of pluripotent embryonic stem cells into cardiomyocytes. Circ Res 2002;91:189–201.
2 Makino S, Fukuda K, Miyoshi S et al. Cardiomyocytes can be generated from marrow stromal cells in vitro. J Clin Invest 1999;103:697–705.
3 Orlic D, Kajstura J, Chimenti S et al. Bone marrow cells regenerate infarcted myocardium. Nature 2001;410:701–705.
4 Tomita S, Li RK, Weisel RD et al. Autologous transplantation of bone marrow cells improves damaged heart function. Circulation 1999;100:II247–II256.
5 Asahara T, Murohara T, Sullivan A et al. Isolation of putative progenitor endothelial cells for angiogenesis. Science 1997;275:964–967.
6 Tsuji H, Miyoshi S, Ikegami Y et al. Xenografted human amniotic membrane-derived mesenchymal stem cells are immunologically tolerated and transdifferentiated into cardiomyocytes. Circ Res 2010;106:1613–1623.
7 Terai M, Uyama T, Sugiki T et al. Immortalization of human fetal cells: The life span of umbilical cord blood-derived cells can be prolonged without manipulating p16INK4a/RB braking pathway. Mol Biol Cell 2005;16:1491–1499.
8 Takeda Y, Mori T, Imabayashi H et al. Can the life span of human marrow stromal cells be prolonged by bmi-1, E6, E7, and/or telomerase without affecting cardiomyogenic differentiation? J Gene Med 2004;6:833–845.
9 Hida N, Nishiyama N, Miyoshi S et al. Novel cardiac precursor-like cells from human menstrual blood-derived mesenchymal cells. Stem Cells 2008;26:1695–1704.
10 Nishiyama N, Miyoshi S, Hida N et al. The significant cardiomyogenic potential of human umbilical cord blood-derived mesenchymal stem cells in vitro. Stem Cells 2007;25:2017–2024.
11 Okamoto K, Miyoshi S, Toyoda M et al. 'Working' cardiomyocytes exhibiting plateau action potentials from human placenta-derived extraembryonic mesodermal cells. Exp Cell Res 2007;313:2550–2562.
12 Grauss RW, Winter EM, van Tuyn J et al. Mesenchymal stem cells from ischemic heart disease patients improve left ventricular function after acute myocardial infarction. Am J Physiol Heart Circ Physiol 2007;293:H2438–H2447.
13 Hou M, Yang KM, Zhang H et al. Transplantation of mesenchymal stem cells from human bone marrow improves damaged heart function in rats. Int J Cardiol 2007;115:220–228.
14 Chen SL, Fang WW, Ye F et al. Effect on left ventricular function of intracoronary transplantation of autologous bone marrow mesenchymal stem cell in patients with acute myocardial infarction. Am J Cardiol 2004;94:92–95.
15 Hare JM, Traverse JH, Henry TD et al. A randomized, double-blind, placebo-controlled, dose-escalation study of intravenous adult human mesenchymal stem cells (prochymal) after acute myocardial infarction. J Am Coll Cardiol 2009;54:2277–2286.
16 Matsushita K, Wu Y, Okamoto Y et al. Local renin angiotensin expression regulates human mesenchymal stem cell differentiation to adipocytes. Hypertension 2006;48:1095–1102.
17 Iwanami J, Mogi M, Li JM et al. Deletion of angiotensin II type 2 receptor attenuates protective effects of bone marrow stromal cell treatment on ischemia-reperfusion brain injury in mice. Stroke 2008; 39:2554–2559.
18 Ikegami Y, Miyoshi S, Nishiyama N et al. Serum-independent cardiomyogenic transdifferentiation in human endometrium-derived mesenchymal cells. Artif Organs 2010;34:280–288.
19 Shinmura D, Togashi I, Miyoshi S et al. Pretreatment of human mesenchymal stem cells with pioglitazone improved efficiency of cardiomyogenic transdifferentiation and improved cardiac function. Stem Cells 2010 (in press).
20 Kami D, Shiojima I, Makino H et al. Gremlin enhances the determined path to cardiomyogenesis. PLoS One 2008;3:e2407.
21 Gnecchi M, He H, Liang O et al. Paracrine action accounts for marked protection of ischemic heart by Akt-modified mesenchymal stem cells. Nat Med 2005;11:367–368.

See www.StemCells.com for supporting information available online.

SCIENTIFIC REPORTS

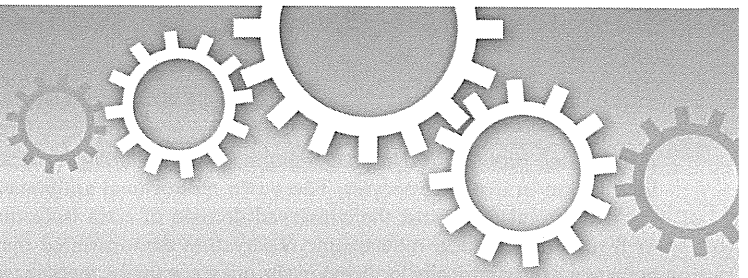

SUBJECT AREAS:
BIOLOGICAL SCIENCES
CELL BIOLOGY
MEDICAL RESEARCH
DEVELOPMENTAL BIOLOGY

Received
8 April 2011

Accepted
4 August 2011

Published
19 August 2011

Correspondence and requests for materials should be addressed to K.M. (kmiyado@nch.go.jp)

* These authors equally contributed to this work

β-catenin is a molecular switch that regulates transition of cell-cell adhesion to fusion

Youki Takezawa[1]*, Keiichi Yoshida[1]*, Kenji Miyado[1], Masahiro Sato[2], Akihiro Nakamura[1], Natsuko Kawano[1], Keiichi Sakakibara[1], Takahiko Kondo[1], Yuichirou Harada[1], Naoko Ohnami[1], Seiya Kanai[1], Mami Miyado[1], Hidekazu Saito[3], Yuji Takahashi[3], Hidenori Akutsu[1] & Akihiro Umezawa[1]

[1]Department of Reproductive Biology, National Center for Child Health and Development, 2-10-1 Okura, Setagaya, Tokyo 157-8535, Japan, [2]Section of Gene Expression Regulation, Frontier Science Research Center, Kagoshima University, 1-21-20 Korimoto, Kagoshima, Kagoshima 890-0065, Japan, [3]Division of Reproductive Medicine, Department of Perinatal Medicine and Maternal Care, National Center for Child Health and Development, 2-10-1 Okura, Setagaya, Tokyo 157-8535, Japan.

When a sperm and an oocyte unite upon fertilization, their cell membranes adhere and fuse, but little is known about the factors regulating sperm-oocyte adhesion. Here we explored the role of β-catenin in sperm-oocyte adhesion. Biochemical analysis revealed that E-cadherin and β-catenin formed a complex in oocytes and also in sperm. Sperm-oocyte adhesion was impaired when *β-catenin*-deficient oocytes were inseminated with sperm. Furthermore, expression of β-catenin decreased from the sperm head and the site of an oocyte to which a sperm adheres after completion of sperm-oocyte adhesion. UBE1-41, an inhibitor of ubiquitin-activating enzyme 1, inhibited the degradation of β-catenin, and reduced the fusing ability of wild-type (but not *β-catenin*-deficient) oocytes. These results indicate that β-catenin is not only involved in membrane adhesion, but also in the transition to membrane fusion upon fertilization.

An oocyte fuses to only one sperm at fertilization, which results in the creation of a single cell with two nuclei that undergoes a series of complex processes (Supplementary Fig. S1a)[1]. After the sperm detaches the cumulus cells, the somatic cells surrounding oocytes, from the oocytes by enzymatic activities, the sperm adheres to the zona pellucida (ZP), the oocyte extracellular matrix. The sperm then penetrates the ZP and adheres to the oocyte cell membrane. At this time, fusion occurs between sperm and oocyte.

CD9[2] and Izumo1[3] belong to the tetraspan protein family (tetraspanin) and immunoglobulin superfamily, respectively, and play a crucial role in sperm-oocyte fusion[3–5]. Both *CD9*-deficient oocytes and *Izumo1*-deficient sperm are unable to fuse to their wild-type partner's cells, but retain adhesive activity[3,4]. A couple of these findings suggest that the molecular event underlying membrane adhesion is different from that underlying membrane fusion. The mechanism of membrane fusion has been explored by us[6] and others[7,8], but little is known about the factors regulating the adhesion of a sperm to an oocyte membrane.

Three proteins, β-catenin, α-catenin and E-cadherin, are a well-known functional set mediating intercellular junctions, which are called adherens junctions and typically served as a lateral connector between epithelial cells[9]. Besides epithelial cells, these three proteins are co-expressed in non-epithelial female germ cells, such as immature oocytes and fully-grown oocytes (to which only one sperm can adhere upon fertilization)[10]. Typically, β-catenin directly binds to the cytoplasmic domain of E-cadherin and connects to the adherens junctional complex with actin, a major component of microfilaments[11]. The β-catenin bound to E-cadherin is involved in intercellular adhesion, while E-cadherin-free β-catenin functions as a transcriptional factor driving the Wnt signaling pathway that regulates embryonic morphogenesis[12].

In mouse oocytes, the presence of both β-catenin and E-cadherin has been reported[10], but it remains unclear whether these two proteins are essential during the process of fertilization. In this study, we explored the possible role of β-catenin in sperm-oocyte adhesion, one of the important steps leading to mammalian fertilization.

Results

Subcellular localization of actin and its possible function in sperm-oocyte adhesion. To identify candidate proteins involved in sperm-oocyte membrane adhesion, we first examined immunocytochemically whether two

cytoskeletal proteins, actin and tubulin, would exhibit cortical localization in ovulated oocytes. These two monoclonal antibodies (mAbs) are raised against the conserved domain of actin isoforms or β-tubulin. Confocal microscopic observation demonstrated that actin was asymmetrically localized in the oocyte: namely, metaphase II-arrested chromosomes enclosed by the actin were observed in one side of the oocyte cytoplasm (Supplementary Fig. S1b, c). In addition, actin was found to be concentrated on the cortical surface of the oocyte and appeared to exist as orderly arranged spots beneath the oocyte cell membrane (Supplementary Fig. S1d). Since tetraspanin CD9 is known to be present on the microvilli that regularly line the cell surface of an oocyte[8], oocytes were subjected to double staining with CD9 and actin mAbs. Neither protein was co-localized, and the actin-rich cortical area was clearly separated from the CD9-rich area (Supplementary Fig. S1d, e), implying the presence of at least two types of membranous structures in the oocyte cell membrane, as suggested previously[13]. Since CD9 plays an important role in sperm-oocyte fusion, but not sperm-oocyte adhesion[4], it was hypothesized that the actin-rich membranous structure on the cell surface of an oocyte may be involved in sperm-oocyte membrane 'adhesion'.

E-cadherin/β-catenin complex formation in both oocytes and sperm. Since E-cadherin/β-catenin complex has been known to bind to actin, by which cell-cell membrane adhesion is regulated[9], we considered that this E-cadherin/β-catenin complex may play a role as a regulator of sperm-oocyte membrane adhesion. To assess the problem, we first examined the possible interaction between E-cadherin/β-catenin complex and actin on an oocyte using immunocytochemical methods. In Fig. 1, subcellular localization of α- and β-catenins and E-cadherin is shown and data on the

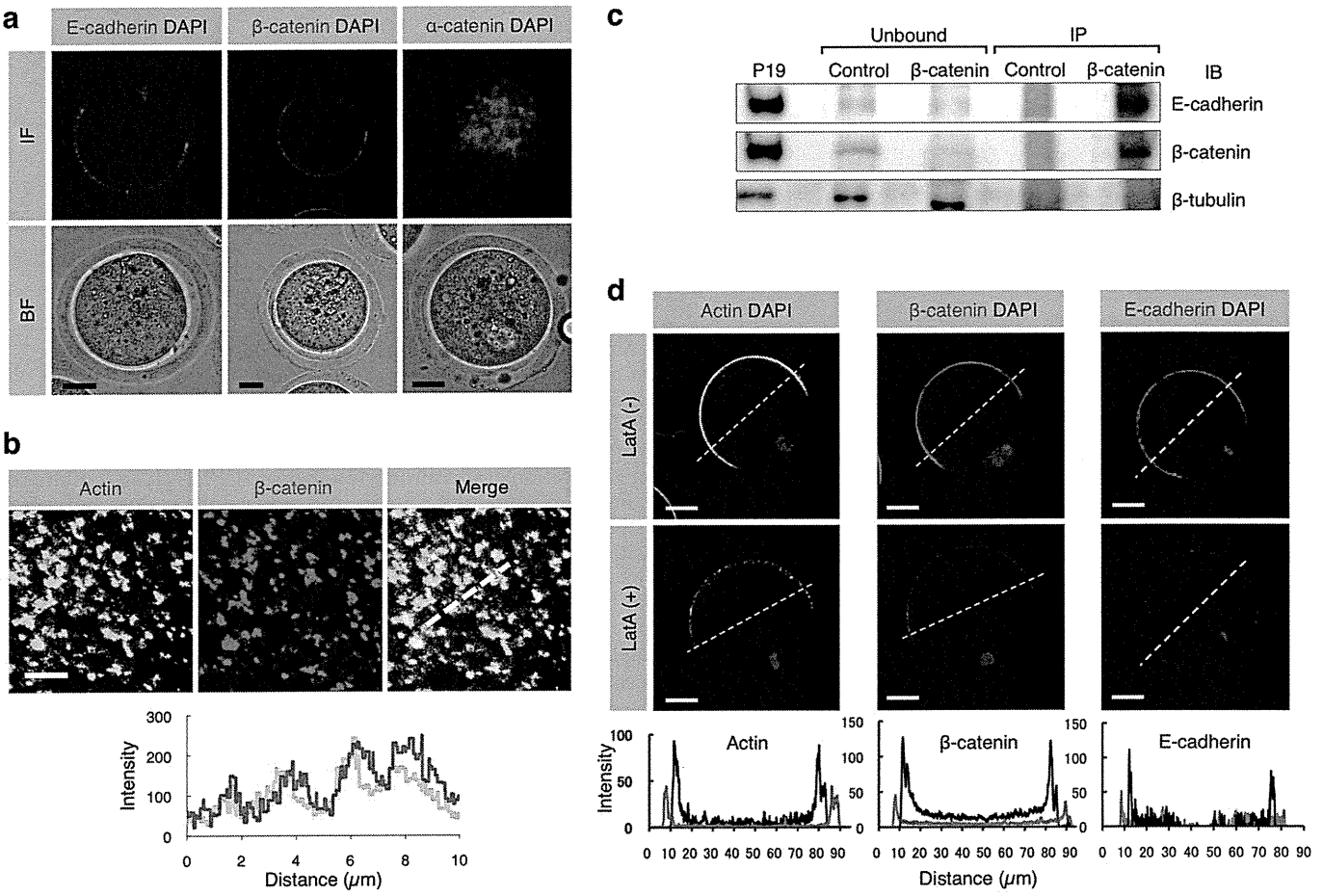

Figure 1 | Expression of E-cadherin and β-catenin and localization of E-cadherin/β-catenin complex in oocytes. (a) Localization of E-cadherin, β-catenin and α-catenin in ovulated oocytes. Similar distribution pattern of E-cadherin and β-catenin on an oocyte suggests complex formation between these two proteins. IF, immunofluorescence; BF, bright field. Scale bars: 20 μm. (b) Localization of β- and γ-actin isoforms and β-catenin beneath the oocyte cell membrane and their fluorescent intensities. The route scanned on the membrane was indicated as a dotted line. Fluorescence intensities for each protein were measured and graphed based on the 3D image, as described in the Experimental Procedures. Red and green lines in the lower panel indicate intensities of β-catenin and actin, respectively. Scale bar: 5 μm. (c) Biochemical evidence for the presence of E-cadherin/β-catenin complex in oocytes. The extract from 905 oocytes immunoprecipitated (IP) by anti-β-catenin mAb and mouse IgG purified from preimmune serum (Control) was subjected to immunoblotting with anti-E-cadherin, anti-β-catenin or anti-β-tubulin mAb. Extracts from mouse embryonic carcinoma cell line P19[35] were also subjected to immunoprecipitation with anti-β-catenin mAb and the resulting immunoprecipitates were reacted with each mAb as a positive control. Note that the extract (IP) immunoprecipitated by anti-anti-β-catenin mAb was reactive with both anti-β-catenin and anti-E-cadherin mAbs, but the extract (Unbound) that was not immunoprecipitated by anti-β-catenin mAb failed to bind to both antibodies. On the other hand, the β-tubulin was detectable in the Ab-unbound (but not Ab-IP) fractions. (d) Disassembly of β-catenin, E-cadherin and actin induced by latrunculin A (latA) treatment. Oocytes were doubly immunostained with anti-β- and γ-actin isoforms mAbs and DAPI (shown as 'Actin DAPI') or with anti-β-catenin mAb or with anti-E-cadherin mAb and DAPI (shown as 'β-catenin DAPI' or 'E-cadherin DAPI'). In the lower panels, the fluorescence intensities measured after being traced along dotted lines in the figures of the upper panels are shown. The intensities of latA-treated oocytes are indicated by red lines, while those of the latA-untreated oocytes are shown by black lines. Scale bar: 20 μm.

comparison between their localization and the localization of actin is also shown. Regarding the immunoreactivity of E-cadherin to an oocyte, a mAb that recognizes an N-terminal extracellular region of E-cadherin was used. Immunocytochemical staining demonstrated that E-cadherin was localized on the cell membrane (microvillar region) of an oocyte that has not been treated with permeabilization (Fig. 1a). β-catenin was detected beneath the oocyte cell membrane, and its localization pattern appeared to be similar to that of E-cadherin (Fig. 1a). In contrast, α-catenin was present in the oocyte cytoplasm (Fig. 1a). When the distribution of β-catenin on an oocyte was compared to that of actin, both proteins were found to be co-localized (Fig. 1b).

Secondly, we assessed the possible formation of β-catenin and E-cadherin complex using an immunoprecipitation method. A cell extract of mouse oocytes (n = 905) was immunoprecipitated with anti-E-cadherin mAb, and the resulting precipitate was then reacted with anti-β-catenin mAb. As a result, the cell extract immunoprecipitated with anti-E-cadherin mAb reacted with the anti-β-catenin mAb (Fig. 1c), indicating the presence of β-catenin and E-cadherin complex in an oocyte.

Thirdly, we assessed the effect of latrunculin A (latA), an inhibitor of actin polymerization, on the formation of β-catenin and E-cadherin complex. When oocytes were treated with 10 μM latA for 1 h at 37°C, actin immunoreactivity was reduced along with decreased immunoreactivity to β-catenin and E-cadherin (Fig. 1d). These results suggest that the β-catenin/E-cadherin complex formed in the oocyte cell membrane is closely associated with actin.

Since the β-catenin/E-cadherin complex is known to play a role in cell-cell adhesion via its homophilic interaction with E-cadherin[14], we predicted that this protein complex would also be produced in sperm. To test this hypothesis, epididymal capacitated sperm were collected from 10-week-old males and subjected to Western blotting (Fig. 2a) and immunoprecipitation (Fig. 2b) analyses. Western blotting revealed that both E-cadherin and β-catenin were detected in the sperm collected (Fig. 2a); however, N-cadherin was not detectable in those samples (Fig. 2a), although its expression has been reported in mouse oocytes[15]. Immunoprecipitation analysis also revealed the presence of the E-cadherin/β-catenin complex in sperm. The sperm extracts immunoprecipitated with anti-β-catenin mAb were reactive with anti-E-cadherin mAb, and those immunoprecipitated with anti-E-cadherin mAb were reactive with anti-β-catenin mAb (Fig. 2b). To confirm this further, immunocytochemical staining was performed for the isolated sperm. Staining of unpermeabilized sperm with anti-E-cadherin mAb demonstrated that E-cadherin was broadly expressed on the cell membrane of sperm from the head region to the mid-piece as well as part of the tail (Fig. 2c, d). Staining of permeabilized sperm with anti-β-catenin mAb revealed that the expression of β-catenin was localized beneath the sperm cell membrane and, notably, its localization pattern was similar to that of E-cadherin (Fig. 2c, d).

In mammals, both sperm-oocyte fusion and adhesion have been believed to occur in a specific region of the sperm head, called an equatorial segment (ES)[1]. Therefore, it is reasonable to consider that factor(s) regulating sperm-oocyte adhesion should exist in this segment. Since in the sperm head of the Asian musk shrew, *Suncus murinus*, ES is recessed within the waist of the sperm nucleus[16], it is easy to detect proteins localized in this segment. When immunocytochemical staining of the permeabilized shrew capacitated sperm was performed using anti-E-cadherin mAb, E-cadherin was expressed on the ES, the mid-piece and part of the tail (Supplementary Fig. S2a). Staining with anti-β-catenin mAb revealed the expression of β-catenin specifically localized on the ES of the sperm head (Supplementary Fig. S2b). Notably, its localization pattern was similar to that of E-cadherin in the shrew sperm (Supplementary Fig. S2a *vs.* Fig. S2b) and also to that of E-cadherin in the mouse sperm (Fig. 2c, d). Furthermore, some β-catenin molecules were released from the acrosomes of the shrew sperm (Supplementary Fig. S2b). Since the ES is recessed in the acrosome of the shrew sperm[16], β-catenin may have accumulated specifically in the ES upon completion of ES formation. These collected results led to a conclusion

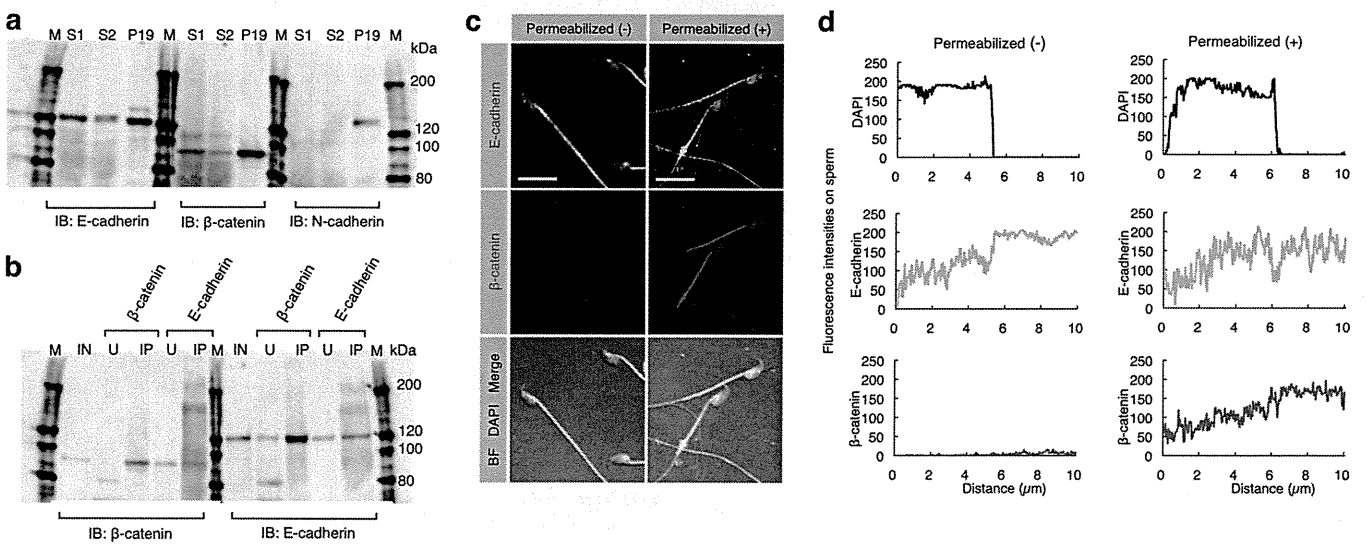

Figure 2 | Expression of E-cadherin and β-catenin and their interaction in sperm. (a) Expression of E-cadherin and β-catenin in epididymal sperm. E-cadherin and β-catenin, but not N-cadherin, in the sperm were detected by immunoblotting (IB). Sperm (S1 and S2) were collected from the epididymis of two males and used for IB. Extracts from P19 cells were used as a positive control. IB was performed using anti-E-cadherin, anti-β-catenin or anti-N-cadherin mAbs. M, molecular weight markers. (b) Interaction between E-cadherin and β-catenin in sperm. Extracts from the sperm (used as input sample (IN)) were immunoprecipitated by anti-E-cadherin or anti-β-catenin mAb. The precipitates (IP) and unbound extracts (U) were immunoblotted (IB) with anti-E-cadherin or anti-β-catenin mAb. M, molecular weight markers. (c) Localization of E-cadherin and β-catenin in sperm. Unpermeabilized or permeabilized sperm were doubly immunostained with anti-E-cadherin (ECCD-2) and anti-β-catenin mAbs, and their nuclei were stained with DAPI. ECCD-2, which recognizes an epitope in the N-terminal extracellular region of E-cadherin, bound to E-cadherin without permeabilization pretreatment. Scale bar: 5 μm. (d) The fluorescence intensity profiles of E-cadherin and β-catenin in sperm shown in (c). Fluorescence intensities were measured after being traced on the sperm along dotted lines shown at the bottom of the panels in (c).

that mammalian epididymal sperm always form E-cadherin/β-catenin complex.

Generation of *β-catenin*-, *α-catenin*- and *E-cadherin*-deficient oocytes. To determine which genes are involved in sperm-oocyte adhesion among *β-catenin*, *α-catenin* and *E-cadherin* genes, three strains (*E-cadherin*$^{floxed/floxed}$ [17], *β-catenin*$^{floxed/floxed}$ [18], and *α-catenin*$^{floxed/floxed}$ [19]) with *loxP*-flanked genes were inter-crossed with the transgenic mouse strain (*Tg*$^{ZP3\text{-}cre/+}$) expressing cre-recombinase in an oocyte-specific manner. Offspring (F2) lacking each type of gene (*E-cadherin*$^{floxed/floxed}$*Tg*$^{ZP3\text{-}cre/+}$, *β-catenin*$^{floxed/floxed}$*Tg*$^{ZP3\text{-}cre/+}$ and *α-catenin*$^{floxed/floxed}$*Tg*$^{ZP3\text{-}cre/+}$) were successfully obtained according to the Menderian inheritance rule (see Methods; Supplementary Fig. S3a), and were all viable and normal in size without displaying any overt physical or behavioral abnormalities. When the number of ovulated oocytes from these superovulated offspring was counted and compared with that of oocytes from the control floxed mice, there were no clear differences in the number of ovulated oocytes between the two groups: 11.7 ± 1.4 (n = 25) for *E-cadherin*$^{floxed/floxed}$*Tg*$^{ZP3\text{-}cre/+}$and 13.7 ± 1.9 (n = 22) for *E-cadherin*$^{floxed/floxed}$; 23.2 ± 1.5 (n = 21) for *β-catenin*$^{floxed/floxed}$*Tg*$^{ZP3\text{-}cre/+}$ and 23.2 ± 1.5 (n = 19) for *β-catenin*$^{floxed/floxed}$; 15.6 ± 2.4 (n = 9) for *α-catenin*$^{floxed/floxed}$*Tg*$^{ZP3\text{-}cre/+}$ and 12.4 ± 2.3 (n = 9) for *α-catenin*$^{floxed/floxed}$. Oocytes isolated from each line carrying the *cre-recombinase* gene were not morphologically distinguishable from those from each control floxed line (Supplementary Fig. S3b). To confirm whether oocytes from these gene-disrupted mice exhibit loss of target protein expression, oocytes were subjected to immunocytochemical staining together with oocytes from control floxed mice. E-cadherin, β-catenin and α-catenin were indeed absent from oocytes of *E-cadherin*$^{floxed/floxed}$*Tg*$^{ZP3\text{-}cre/+}$, *β-catenin*$^{floxed/floxed}$*Tg*$^{ZP3\text{-}cre/+}$ and *α-catenin*$^{floxed/floxed}$*Tg*$^{ZP3\text{-}cre/+}$, respectively (Supplementary Fig. S3b). These results suggest that these three genes are not essential for the maturation and ovulation of mouse oocytes.

In epithelial cells, β-catenin is required for localization of E-cadherin on the cell surface, and endocytosis of E-cadherin into the cytoplasm occurs in the absence of β-catenin[20]. In addition, a model was proposed: α-catenin participates to bind to the E-cadherin/β-catenin complex to connect with actin microfilaments under certain specific conditions[9]. In analogy to this, it is possible that cellular localization of E-cadherin, β-catenin and α-catenin is mutually regulated in oocytes. Such a possibility is already depicted in Fig. 1a, in which E-cadherin was co-localized with β-catenin, but not with α-catenin on a wild-type oocyte. To examine whether the formation of E-cadherin/β-catenin complex (possibly E-cadherin/β-catenin/α-catenin complex) is impaired when either one of these composite proteins is deficient, oocytes collected from all of the gene-ablated strains were immunocytochemically assessed for localization of these three proteins (Supplementary Fig. S4a–c). Expression of E-cadherin was strongly reduced on the cell membrane of *β-catenin*-deficient oocytes, but not *α-catenin*-deficient oocytes (Supplementary Fig. S4a *vs.* Fig. S4b). On the other hand, loss of E-cadherin did not affect the localization pattern of β-catenin and α-catenin (Supplementary Fig. S4c). Similar results were also obtained when *α-catenin*-deficient oocytes were examined (Supplementary Fig. S4a). These results indicate that β-catenin regulates the membrane localization of E-cadherin in mouse oocytes.

Sperm-oocyte adhesion or fusion assay. Membrane interaction between oocytes and sperm occurs after the penetration of sperm into ZP (Supplementary Fig. S1a). To monitor such interaction directly, 'ZP-free' *β-catenin*-deficient oocytes after enzymatic digestion of ZP were inseminated with wild-type epididymal sperm (Fig. 3a, b for adhesion assay; Fig. 3c–e for fusion assay). 'ZP-free' oocytes from *β-catenin*$^{floxed/floxed}$ mice were used as a control. When the oocytes were inspected 1 h after insemination and stained with 4',6-diamidino-2-phenylindole (DAPI) after fixation, as depicted in Fig. 3a, the number of sperm adhered to 'ZP-free' *β-catenin*-deficient oocytes was significantly reduced (Fig. 3b) compared to sperm bound to control oocytes. Similarly, when DAPI-preloaded oocytes were inspected 1 h after insemination, as depicted in Fig. 3c, the relative rate of 'ZP-free' *β-catenin*-deficient oocytes fused with sperm was also significantly reduced (39.2 ± 12.7 *vs.* 100.0 for control oocytes; $P<0.003$; Fig. 3d, e). We next examined the expression pattern of CD9, an essential protein for fusion[4], in *β-catenin*-deficient oocytes immunocytochemically and immunobiochemically to assess the ability of wild-type C57BL/6N sperm to fuse with their membrane. CD9 was expressed on the plasma membrane of 'ZP-free' *β-catenin*-deficient oocytes at a level comparable to that of 'ZP-free' control oocytes (Supplementary Fig. S5a). The total amount of CD9 quantified by immunoblotting in *β-catenin*-deficient oocytes was comparable to that of control oocytes (Supplementary Fig. S5b). These findings suggest that β-catenin is involved in sperm-oocyte adhesion.

***In vitro* fertilizing ability of *β-catenin*-deficient oocytes.** To know how fertilization is influenced by the dysfunction of sperm-oocyte adhesion, we determined the fertilization rate of *β-catenin*-deficient oocytes. The *β-catenin*-deficient oocytes surrounded by cumulus cells (herein referred to as 'cumulus-intact' oocytes) were isolated from oviducts and directly subjected to IVF with wild-type sperm, as depicted in Fig. 3f. 'Cumulus-intact' oocytes from *β-catenin*$^{floxed/floxed}$ mice were used as a control. When the oocytes were inspected 24 h after insemination, the relative rate of *β-catenin*-deficient oocytes fused with sperm was not reduced (Fig. 3g). Quantitative analysis revealed that the rate of *β-catenin*-deficient oocytes fused with sperm was rather enhanced (119.6 ± 4.6 *vs.* 100.0 for control oocytes; $P<0.02$; Fig. 3h), in contrast with the results of the previous adhesion/fusion assay (Fig. 3a–e). This is probably due to the occasional presence of the oocytes fused to sperm, which failed to develop to the two-cell stage; however, the fact that certain embryos developed to the two-cell stage would not exclude the possibility of pathogenetic activation of oocytes. On the other hand, the IVF rate (which is evaluated by the development of fertilized oocytes to the two-cell stage) was comparable between the two groups (Fig. 3i).

We further confirmed the above point by counting litters obtained through mating between *β-catenin*$^{floxed/floxed}$*Tg*$^{ZP3\text{-}cre/+}$ females and *β-catenin*$^{floxed/floxed}$ males. The control *β-catenin*$^{floxed/floxed}$ females were similarly mated. The litter size of *β-catenin*$^{floxed/floxed}$*Tg*$^{ZP3\text{-}cre/+}$ females was 5.3 ± 0.4, which was comparable with that of control females (5.8 ± 0.4) (Supplementary Fig. S6). These results indicate that oocytes lacking β-catenin expression reduce the ability to adhere with sperm, but sustain the ability to fuse with sperm as well as the total reproductive ability needed for delivering pups.

Possible involvement of β-catenin in transition of membrane adhesion to fusion. To examine the dynamics of β-catenin at sperm-oocyte membrane adhesion, alteration in the localization pattern of β-catenin at the sperm attachment sites of the *in vitro* fertilized "zona-free" oocyte was monitored (Fig. 4a–c). Before sperm attachment, β-catenin-rich patches (as shown in Fig. 1b) were clearly detected on the surface of an oocyte (upper left panel of Fig. 4a); however, these patches became undetectable 30 min after sperm attachment (arrows in the lower left panel; Fig. 4a). Furthermore, β-catenin was abundantly present in the capacitated sperm head (upper middle and right panels of Fig. 4a) before sperm attachment, but the amount of β-catenin in sperm heads was also greatly reduced after insemination (arrows in the lower middle and right panels; Fig. 4a). In addition, β-catenin was localized in the sperm head, although its localization pattern was slightly different in each sperm. Notably, β-catenin tended to be concentrated at ES (Fig. 2c; Supplementary Fig. S2; Fig. 4a).

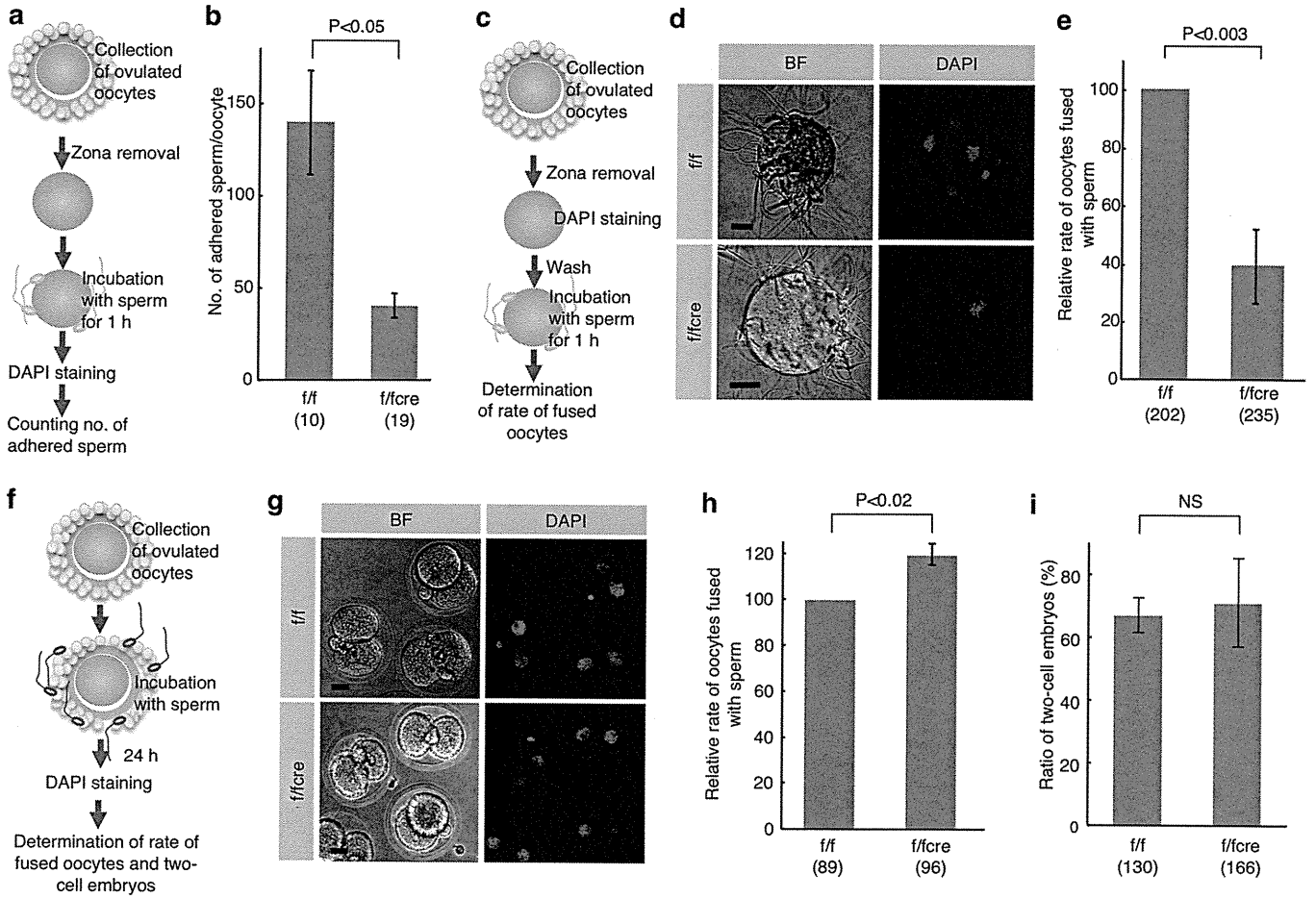

Figure 3 | *In vitro* fertilizing ability of *β-catenin*-deficient oocytes. (a) Experimental flow for testing sperm-oocyte membrane 'adhesion', and comparison of the number of wild-type sperm adhered to an 'zona-free' oocyte between f/fcre and f/f oocytes. After ZP removal, 'zona-free' oocytes were mixed with sperm for 1 h. (b) The number of sperm adhered to an oocyte was counted by DAPI-derived fluorescence in sperm heads on the surface of an oocyte. Parentheses indicate the number of oocytes examined. Values are the mean ± standard error (SE). (c) Experimental flow for testing sperm-oocyte membrane 'fusion' and fused sperm (shown as DAPI-positive sperm) in 'zona-free' *β-catenin*-deficient (f/fcre) and control (f/f) oocytes. After ZP removal, subsequent preincubation for 20 min in the presence of DAPI and washing, 'zona-free' oocytes were mixed with the wild-type sperm for 1 h. (d) Comparison of oocytes fused with sperm between f/fcre and f/f oocytes. BF, bright field. Bars: 20 μm. (e) Comparison of the relative rate of oocytes fused with sperm between f/fcre and f/f oocytes. Only oocytes having at least one fused sperm were counted. The comparative values relative to the control (f/f oocytes; set to 100.0) were displayed as the relative rate of fused oocytes. Parentheses indicate the number of oocytes examined in triplicate experiments. Values are the mean ± SE. (f) Experimental flow for testing sperm-oocyte membrane interaction and fused sperm in two-cell embryos developing from 'cumulus-intact' *β-catenin*-deficient (f/fcre) and control (f/f) oocytes. DAPI staining was performed to detect fused sperm on the developing two-cell embryos. (g) Comparison of oocytes fused with sperm between "cumulus-intact" f/fcre and f/f oocytes. Bars: 20 μm. (h) Comparison of the relative rate of oocytes fused with sperm between "cumulus-intact" f/fcre and f/f oocytes. Parentheses indicate the number of oocytes examined in triplicate experiments. Values are the mean ± SE. (i) Comparison of the ratio of oocytes developing to two-cell stage 24 h after fertilization between "cumulus-intact" f/fcre and f/f oocytes, according to the procedure described in (f). Parentheses indicate the total number of oocytes examined in triplicate experiments. NS, not significant. Values are the mean ± SE.

These findings could also be supported by measurement of fluorescent intensities of β-catenin (Fig. 4b, c). When fluorescence intensity at the equator of an oocyte (dotted line in the upper image of the left panels; Fig. 4a) was compared with that in the region of an oocyte adhered to sperm (dotted line in the lower image of the left panels; Fig. 4a), intense localization of β-catenin in the oocyte exhibiting no sperm attachment was observed beneath the oocyte membrane (arrows in the upper graph; Fig. 4b); however, 30 min after sperm attachment, the fluorescent intensity of β-catenin beneath the oocyte membrane was markedly reduced (arrows in the lower graph; Fig. 4b). Concomitantly, fluorescence intensity throughout the entire sperm (dotted lines in the right panels; Fig. 4a) was quantitatively compared before and after sperm adhesion to the oocyte membrane (Fig. 4c). Before attachment to the oocyte membrane, β-catenin was broadly localized in the sperm head (corresponding to the DAPI-stained region), mid-piece and part of the tail (Fig. 2c, d; upper graph of Fig. 4c); however, after attachment to the oocyte membrane, the intensity of β-catenin in the sperm head (but not in a mid-piece and tail) was markedly decreased (arrows in the lower middle and right panels of Fig. 4a; lower graph of Fig. 4c). Moreover, to confirm that the amount of β-catenin is reduced at steps between sperm-oocyte adhesion and fusion, localization pattern of β-catenin at the sperm attachment sites of the *in vitro* fertilized "zona-free" *CD9*-deficient oocyte was monitored (Fig. 4d, e). Before sperm attachment, intense localization of β-catenin (as shown in the upper left panel of Fig. 4a) was clearly seen on the surface of an oocyte (upper middle panel of Fig. 4d); however, these patches became undetectable 30 min after sperm attachment (arrows in the lower middle panel; Fig. 4d). These findings were also confirmed by measurement of fluorescent intensities of β-catenin (Fig. 4e). When